Improving Anti-PD1 Uptake and Therapy in Tumors Using Acoustic Cluster Therapy (ACT) in Mice

Håkon F. Wesche[1*], Veronica Nordlund[1,3], Oda Natalie Brunstad [1], Petros Yemane[1], Anniken Sjødal[1,4], Einar Sulheim[2], Morten Smedsrud Wigen[2], Ola Finneng Myhre[2], Melina Mühlenpfordt[2], Sofie Snipstad[1,3], Catharina de Lange Davies[1]

[1]Norwegian University of Science and Technology (NTNU), Trondheim, Norway
[2]EXACT Therapeutics AS, Oslo, Norway
[3]Cancer clinic, St. Olav's Hospital – Trondheim University Hospital, Trondheim, Norway
[4]Department of Neurology, St. Olav's Hospital - Trondheim University Hospital, Trondheim, Norway

Immunotherapy, particularly checkpoint inhibitors (ICIs), have substantially improved the treatment outcome for many cancer types. However, the efficacy varies a lot from patient to patient. By improving the delivery of ICIs, tumors may become more responsive to treatment. Acoustic Cluster Therapy (ACT) uses microbubble-microdoplet clusters together with ultrasound sonication to increase local drug delivery to a target tissue. ACT has been shown to increase the uptake and therapeutic efficacy of chemotherapies in various preclinical mouse models. In this work, we study whether ACT can increase tumor uptake of the checkpoint-inhibitor anti-PD1 and improve immunotherapy response.
Immediately after ACT treatment, fluorescent anti-PD1 was intravenously injected and accumulation measured in prostate cancer (PC3) xenografts using small animal optical imaging (IVIS) and microdistribution imaged by confocal microscopy. Next, anti-PD1 uptake and therapy response were assessed in colorectal (CT26) and pancreatic (KPC) syngeneic cancer models. Immune cell infiltration was analyzed by immunofluorescence and confocal imaging to quantify CD8 T cells and neutrophils and relate these measurements to treatment outcomes.
In PC3 tumors, ACT significantly increased anti-PD1 uptake in vivo, confirmed by confocal microscopy. No significant uptake increase was found in CT26 or KPC tumors. Nonetheless, a subset of CT26 and KPC tumors demonstrated improved responses to the combined ACT and anti-PD1 therapy. In the CT26 tumor sections, the aPD1-only and ACT+aPD1 groups showed significantly higher CD8 T cell infiltration than the saline control, while neutrophil levels were unchanged. There was significantly higher neutrophil infiltration in the ACT+aPD1 group compared to saline control in the KPC tumor sections, but no significant differences in the CD8 T cell infiltration. There was no significant correlation between CD8 T cell or neutrophil infiltration and therapeutic outcome in CT26 or KPC tumors.
ACT enhances anti-PD1 tumor uptake in PC3 tumors but not in CT26 or KPC tumors. It is not clear why ACT enhances the anti-PD1 uptake in the human model, but not the murine models. Despite no increased aPD1 uptake, a subset of CT26 and KPC tumors seemed to respond to ACT+anti-PD1 combination therapy. Therefore, further studies are needed to characterize the subset of tumors responding to ACT+aPD1 therapy and elucidate the underlying mechanisms.

Doxorubicin-Loaded Iron Oxide Nanocubes for Targeted Anticancer-Drug Delivery

Egon G. Höfgen[1*], Subastri Ariraman[2], Swathi Sudhakar[2] and Sulalit Bandyopadhyay[1]

[1]Particle Engineering Centre, Department of Chemical Engineering, Norwegian University of Science and Technology, Trondheim, Norway
[2]Department of Applied Mechanics and Biomedical Engineering, Indian Institute of Technology Madras, Chennai, India.

Cancer is a scourge to humankind and annually causes 10 million deaths worldwide.[1] In recent years, the use of nanotechnology in health science has made tremendous progress, evidenced by the increasing numbers of clinically approved platforms spanning from diagnostics to treatment and prevention. Rooted in their biocompatibility and magnetic properties, iron oxide nanoparticles (IONPs) show great potential in the clinical fight against cancer, from imaging to hyperthermia therapy to drug delivery. However, most nanoparticle-based systems are spherical, and the shape specific effects on cells or organisms is overlooked.[2]

Thermal decomposition is a prominent route for synthesizing IONPs of controlled shape and properties, and our work has provided detailed insight into the effects of key parameters in both batch and semi-batch processes.[3] To investigate shape-dependent effects in this present work, we have synthesized cubic IONPs from iron oleate using sodium oleate as shape directing agent. These superparamagnetic nanocubes of around 15 nm edge length, were rendered hydrophilic through oxidative phase transfer and subsequently loaded with the anticancer drug doxorubicin (dox), without altering their cubic morphology confirmed in STEM. Drug loading of up to 400 $\mu mol_{dox}/mg_{IONP}$ was achieved through simple adsorption, in the same range as previous reports of spherical carboxylic-IONPs. Our dox-loaded nanocubes exhibit cytotoxicity towards breast cancer cells (MCF-7), whereas bare IONPs without drug showed no adverse effects.

These results align with our recent findings that cubic IONPs loaded with another anti-cancer drug outperform spherical or platelet-shaped particles.[4] Together, the data highlights the critical role of nanoparticle morphology in designing drug-delivery platforms and point to promising therapeutic potential when combined with magnetic targeting or hyperthermia.[5]

[1] World Health Organization. *Noncommunicable diseases -Fact sheet*. https://www.who.int/news-room/fact-sheets/detail/noncommunicable-diseases (accessed 2025-12-22).
[2] Tollemeto, M. and Lammers, T. The Importance of Particle Shape in Drug Delivery. *Nat Rev Bioeng* **2026**, 1–3.
[2] Höfgen, E. G.; Bandyopadhyay, S. Insights into Semi-Continuous Synthesis of Iron Oxide Nanoparticles (IONPs) via Thermal Decomposition of Iron Oleate. *Discover Nano* **2025**, *20* (1), 5.
[4] Babunagappan, K. V. *et al.* Geometry-Guided Cancer Therapy: Shape-Dependent Uptake and Cytotoxicity of Iron Oxide Nanoparticles. *In submission*
[5] E.H. thankfully acknowledges funding through INCP2 (Indo-Norway Cooperation Program): Fostering Safety in Use of Advanced Nanomaterials in Health Sector funded by Norwegian Directorate for Higher Education and Skills, Norway and University Grants Commission, India

Contributed Talk 03 Dishiti Gupta

Taper-Engineered AlGaN/GaN Nanowire Photonic Crystal Surface-Emitting UV Lasers

Dishiti Gupta, Tron Arne Nilsen, Astrid Aksnes, Bjørn-Ove Fimland and Helge Weman*
Department of Electronic Systems, Norwegian University of Science and Technology (NTNU), NO-7491 Trondheim, Norway

Ultraviolet (UV) solid-state light sources are of growing importance for applications in water purification, surface sterilization, biomedical diagnostics, and chemical sensing. AlGaN/GaN nanowire (NW) photonic crystal (PhC) arrays are a particularly promising platform for realizing compact, efficient UV surface-emitting lasers, owing to the ability of NWs to accommodate lattice mismatch through lateral strain relaxation, suppress threading dislocations, and provide periodic dielectric structuring that supports Γ-point lasing modes with near-zero group velocity. However, a central challenge in these structures is achieving strong vertical light extraction without compromising optical confinement within the NW cavity, a trade-off that fundamentally limits device performance as demonstrated in our previous work with cylindrical NWs [1].

In this work, we present a comprehensive three-dimensional electromagnetic study of taper-engineered AlGaN/GaN NW PhC lasers operating in the UV spectral range. Using full-wave finite-difference time-domain (FDTD) simulations, we systematically analyze the influence of taper height and taper angle on two key figures of merit: the surface outcoupling efficiency (SOE_{abs}) and the Q-factor, both evaluated under realistic material absorption conditions. The results reveal a pronounced quasi-periodic dependence of device performance on the taper geometry, arising from Fabry-Pérot-like resonances along the taper axis whose phase condition evolves continuously with taper height. A physical model based on the energy distribution of the PhC mode and its diffracted components (H_x, H_y) is developed to explain the loss mechanisms and identify geometric configurations that simultaneously maximize surface emission and preserve optical confinement.

Optimized tapered structures demonstrate significant improvements over non-tapered cylindrical geometries. Taper engineering also reduces the Al content required in the lower cladding layer from 50% to 30%, which directly alleviates the electrical conductivity penalty associated with high-Al AlGaN layers, a critical consideration for electrically injected UVB and UVC devices. These findings establish NW tapering not as a passive growth artifact but as a powerful and controllable design parameter, offering a practical pathway toward high-performance AlGaN/GaN NW PhC surface-emitting lasers across the UV spectral range.

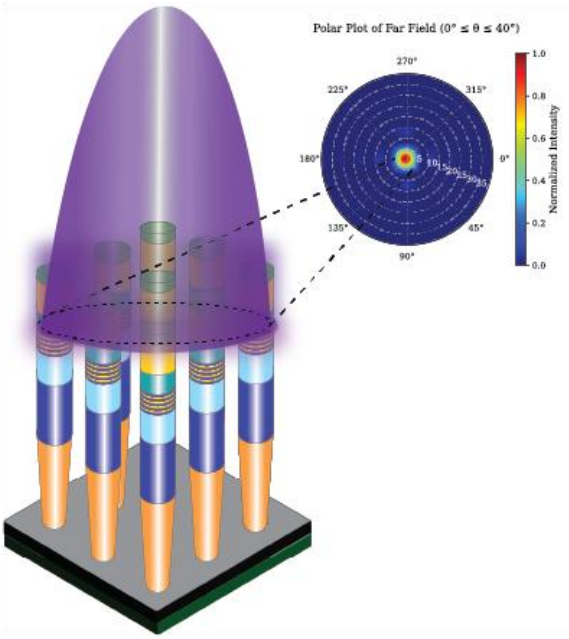

Figure 1: UV emission from AlGaN/GaN NW PhC laser with the far-field plot for the emission.

References

1. D. Gupta, T. A. Nilsen, A. Aksnes, B. -O. Fimland and H. Weman, "Optimization of Surface-Emitting UV Nanowire Photonic Crystal Lasers: A Simulation-Driven Approach," *IEEE Photonics J.*

Hybrid antiferroelectric–ferroelectric-ferroelastic domain walls in noncollinear antipolar oxides

Ivan N. Ushakov[1*], Mats Topstad[2], Muhammad Z. Khalid[1], Niyorjyoti Sharma[3], Christoph P. Grams[4], Ursula Ludacka[1], Jiali He[1], Kasper A. Hunnestad[1,5], Mohsen Sadeqi-Moqadam[1], Julia Glaum[1], Sverre M. Selbach[1], Joachim Hemberger[4], Petra Becker[6], Ladislav Bohatý[6], Amit Kumar[3], Jorge Íñiguez-González[7,8], Antonius T. J. van Helvoort[2], Dennis Meier[1,9,10]

[1]Department of Materials Science and Engineering, Norwegian University of Science and Technology (NTNU), Trondheim, Norway.
[2]Department of Physics, Norwegian University of Science and Technology (NTNU), Trondheim, Norway.
[3]Centre for Quantum Materials and Technologies (CQMT), Queen's University Belfast, Belfast, UK.
[4]Institute of Physics II, University of Cologne, Cologne, Germany.
[5]Department of Electronic Systems, Norwegian University of Science and Technology (NTNU), Trondheim, Norway.
[6]Institute of Geology and Mineralogy, University of Cologne, Cologne, Germany.
[7]Smart Materials Unit, Luxembourg Institute of Science and Technology (LIST), Esch/Alzette, Luxembourg.
[8]Department of Physics and Materials Science, University of Luxembourg, Belvaux, Luxembourg.
[9]Faculty of Physics and Center for Nanointegration Duisburg-Essen (CENIDE), University of Duisburg-Essen, Duisburg, Germany.
[10]Research Center Future Energy Materials and Systems, Research Alliance Ruhr, Bochum, Germany.

Antiferroelectrics are emerging as advanced functional materials with unique electric properties enabled by the antipolar arrangement of their electric dipoles. Additional functionalities and novel physical nanoscale phenomena are expected in systems with noncollinear antipolar dipole structures. Here we demonstrate how the onset of antiferroelectricity in $K_3[Nb_3O_6](BO_3)_2$ drives noncollinear ordering of electric dipole moments, which leads to unusual hybridization of antiferroelectric and ferroelectric responses. Besides the double-hysteresis loop common to antiferroelectrics, a pronounced piezoresponse and electrically switchable hybrid domains are observed using scanning probe microscopy. Scanning transmission electron microscopy shows that the domains are separated by atomically sharp and micrometer-long charged domain walls with inseparably entangled discontinuities in the antiferroelectric and ferroelectric orders. Hybrid antiferroelectric‑ferroelectric responses are expected in a wide range of noncollinear systems.

Investigating the Connection Between Surface Topography, Cell Membrane and Nucleus Deformation and its Impact on Chromatin Organization

Sara Beate S. Årbogen[1] Pawel Sikorski[1] Jonas Paulsen[2] Cinzia A.M. Progida [2]

[1]Department of Physics, NTNU, [2]Department of Biosciences, UiO

The field of mechanobiology explores how physical forces and mechanical properties of cells and tissues impact cell development and cell differentiation in health and disease[1]. Physical forces acting on the cell can lead to perturbation of the cell membrane, causing remodeling of the cytoskeleton which can result in reorganization of the nuclear morphology[2]. This is often associated with chromatin reorganization and changes in gene expression[3]. Unraveling the mechanism of mechanical signaling is challenging because it is difficult to study in a controlled manner. Nanofabrication methods enable the generation of precisely engineered surfaces. When combined with advanced microscopy techniques, they can facilitate controlled and systematic studies of the relationships between mechanical forces, nuclear deformation, and chromatin organization. To achieve this we fabricate nanopillar arrays on glass cover slips using electron beam lithography (Figure 1). Using our sample design we can test three variations of the same parameterer within a single experiment, alongside a flat control region for comparison. By seeding cells onto the substrate and allowing them to adhere, we can observe how their interaction with the nanopillars alters nuclear morphology and chromatin organization through advanced microscopy techniques (Figure 1). We will assess the changes in nuclear morphology and look at changes in HP1-α aggregates in the nucleus, which are proteins that are involved in compaction of chromatin[4]. For future work we aim to include alternative fabrication techniques, which may enable fabrication of more complex surface topography.

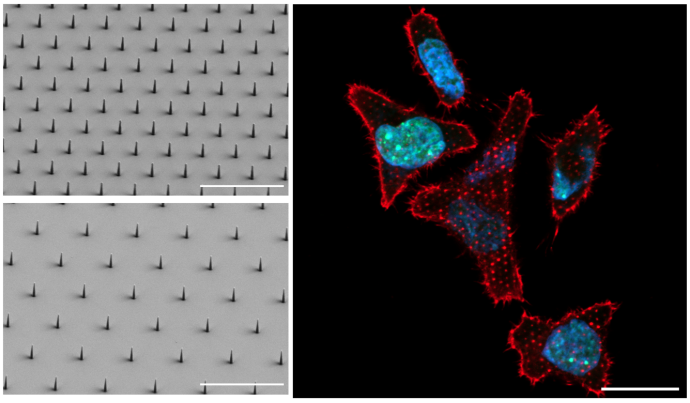

Figure 1: The left panel display SEM images of nanopillars on glass coverslip surface. Each pillar is 1 μm tall and the pillar-to-pillar distance is 2μm in the top image, 3μm in the lower image. Scale bar is 5 μm. To the right is a confocal microscopy image of HeLa cells on top of pillars, with pillar-to-pillar distance of 2μm. HeLa cells express HP1-α GFP (green) and the actin (red) is labeled with AF 647 - Phalloidin, while the DNA is labeled with Hoechst (blue). Scale bar is 20 μm.

References

[1] Danahe Mohammed et al. “Innovative Tools for Mechanobiology: Unraveling Outside-In and Inside-Out Mechanotransduction”. English. In: *Frontiers in Bioengineering and Biotechnology* 7 (July 2019). Publisher: Frontiers. DOI: 10.3389/fbioe.2019.00162.

[2] Caroline Uhler and G. V. Shivashankar. “Chromosome Intermingling: Mechanical Hotspots for Genome Regulation”. In: *Trends in Cell Biology*. Special Issue: Cell Communication 27.11 (Nov. 2017), pp. 810–819. DOI: 10.1016/j.tcb.2017.06.005.

[3] Zeinab Jahed and Mohammad Rk Mofrad. “The nucleus feels the force, LINCed in or not!” en. In: *Current Opinion in Cell Biology* 58 (June 2019), pp. 114–119. DOI: 10.1016/j.ceb.2019.02.012.

[4] Jieqiong Lou et al. “Heterochromatin protein 1 alpha (HP1) undergoes a monomer to dimer transition that opens and compacts live cell genome architecture”. In: *Nucleic Acids Research* 52.18 (Oct. 2024), pp. 10918–10933. DOI: 10.1093/nar/gkae720.

Acoustofluidic trapping of microplastics using travelling surface acoustic waves (TSAW)

Ibrahim Ali[*1], Hamed Salmani[1], Agne Johannessen[1], Einar Halvorsen[1], Ulrik Hanke[1]*

[1]Department of Microsystems, University of South-Eastern Norway (USN), Norway

Microplastics (MPs) are an increasing environmental concern, and current characterization techniques remain limited in their ability to identify individual particles smaller than 20 µm. This project aims to quantify MPs using an acoustofluidic trapping approach integrated with sensing. The current phase focuses on developing a simulation model for a travelling surface acoustic wave (TSAW)-based trapping system proposed by Destgeer et al.[1] and validating it against experimental measurements. Figure 1 illustrates the TSAW-based microfluidic device, experimental trapping results, and simulated particle trajectories. This work serves as an initial step toward the final project goal of developing an integrated portable solution for real-time monitoring of MPs in aqueous media.

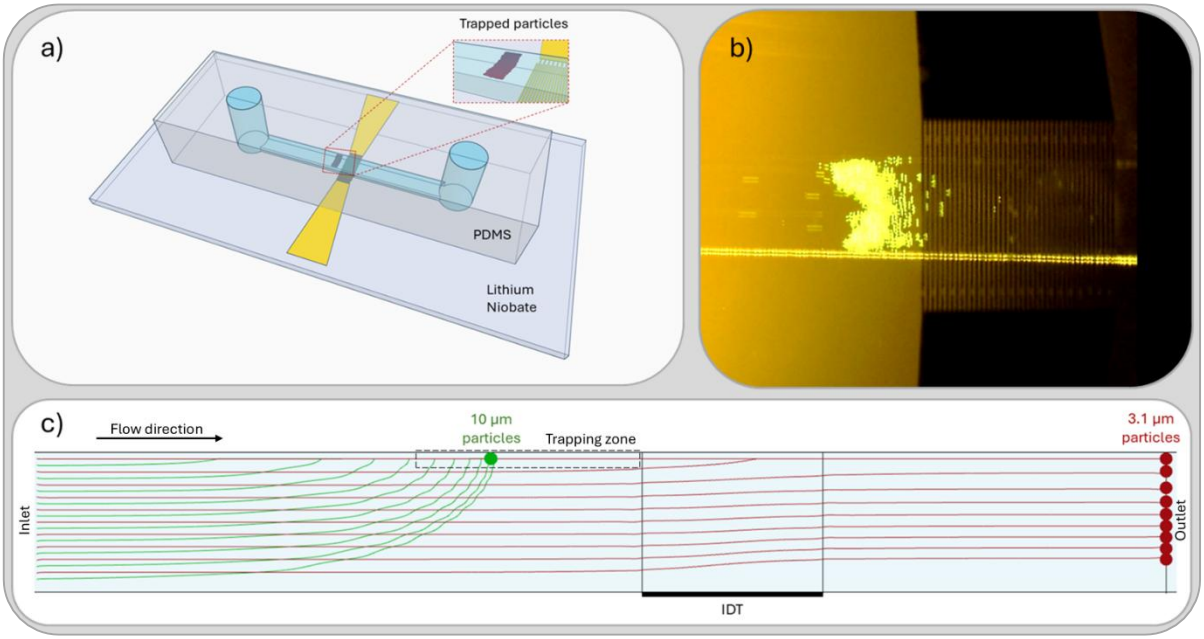

Figure 1. (a) Schematic of the TSAW-based microfluidic device for microplastic trapping. (b) Experimental trapping of 10 µm polystyrene particles in the microchannel. (c) 2D COMSOL simulation of particle trajectories for 10 µm and 3.1 µm particles, showing size-selective trapping under TSAW actuation (vertical axis is enlarged by a factor of 7 for visualization).

[1] G. Destgeer, A. Hashmi, J. Park, H. Ahmed, M. Afzal, and H. J. Sung, "Microparticle self-assembly induced by travelling surface acoustic waves," RSC Adv., vol. 9, no. 14, pp. 7916–7921, 2019, doi: 10.1039/C8RA09859J.

Surface-Adsorbed Water as a Limiting Loss Mechanism in Mid-Infrared Photonics

Antonia Torres-Cubillo[1,2], Martin Feiler[1,3], Roman Zakoldaev[1], Jehona Salaj[1], Noémie Mestre[1], Sebastián Alberti[1], Henock D. Yallew[1], and Jana Jágerská[1]

[1] UiT The Arctic University of Norway, NO-9037 Tromsø, Norway
[2] University of Málaga, 29010 Málaga, Spain
[3] Slovak University of Technology in Bratislava, 81219 Bratislava, Slovakia
noemie.mestre@uit.no

Minimizing optical loss is central to advancing mid-infrared (mid-IR) photonics for applications in sensing, spectroscopy, and on-chip integration. In this work, we will discuss surface-adsorbed water [1] as a fundamental and often overlooked loss channel in mid-IR photonic devices. We demonstrate that even nanometer-scale water layers on photonic surfaces can introduce substantial absorption in the mid-IR, and particularly around the water absorption peaks around 3 and 6 µm. Humidity-induced loss in different air-clad mid-IR waveguide designs [2,3] is quantified experimentally and reproduced in simulations, revealing critical excess attenuation exceeding 10 dB/cm at 3.27 µm. Measurable attenuation of the order of 0.2 dB/cm is, however, present even in water absorption window at 4.35 µm. While hydrophobic surfaces mitigate the problem, they do not fully suppress it, indicating that no simple technological solution currently exists. Addressing this challenge is essential for enabling truly low-loss MIR photonic integrated circuits.

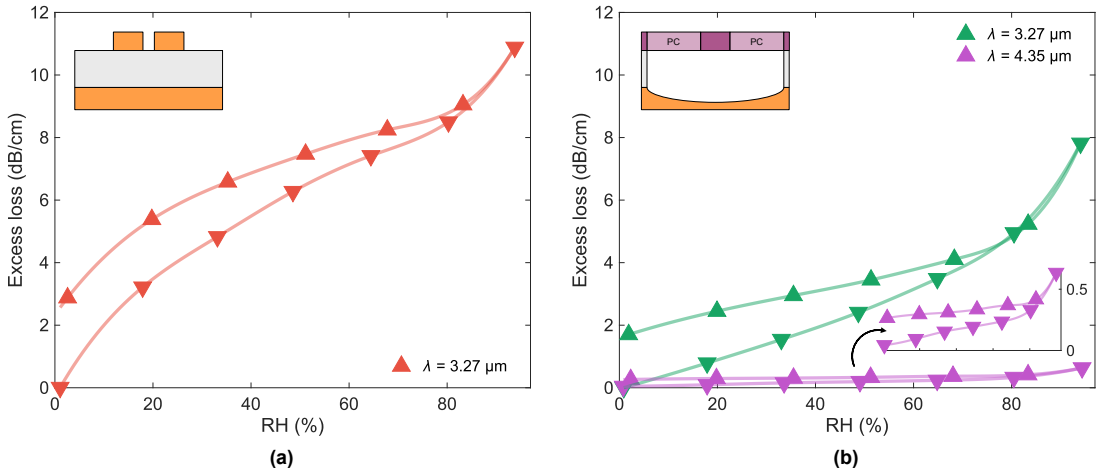

Fig. 1. Humidity-induced excess loss. Adsorption–desorption hysteresis curves for a (a) SOI slot waveguide and (b) suspended thin-film SiN waveguides at two MIR wavelengths.

References

[1] L. Chen *et al.*, "Water Adsorption on Hydrophilic and Hydrophobic Surfaces of Silicon," *J. Phys. Chem. C.*, vol. 122, no. 21, pp. 1385-11391, 2028, DOI: 10.1021/acs.jpcc.8b01821.
[2] J. Salaj, M. Vlk, R. Zakoldaev, R.Seton, J. Čtyroký, S.Alberti, A.Aksnes, and J. Jágerská, *Suspended nanophotonic waveguide for isotope-specific CO_2 detection*, Optica 11, 1654-1662 (2024)
[3] H. D. Yallew *et al.*, "Sub-ppm Methane Detection with Mid-Infrared Slot Waveguides," *ACS Photonics*, vol. 10, no. 12, pp. 4282–4289, Dec. 2023, DOI: 10.1021/acsphotonics.3c01085.

This work was supported by the European Research Council (Proof of Concept grant No. 101158155), the European Innovation Council Pathfinder Open (grant No. 101128598), and by the Research Council of Norway (project No. 295864). The authors thank Marek Vlk for valuable discussions and insights.

Deposition and characterization of novel oxide perovskites

Anjali Choubey *, Ola Nilsen, Holger von Wenckstern, Henrik Hovde Sønsteby
Center for Materials Science and Nanotechnology, University of Oslo, Norway
*anjalic@uio.no

Rare-earth oxide perovskites exhibit robust crystal chemistry and rich functional behaviour, including metal-insulator transitions, strong electron-lattice coupling, and complex magnetic order, making them attractive for sensing, spintronics, optoelectronics, and other energy-related devices. Several rare-earth nickelates show electronic and magnetic phase transitions and are highly tunable by strain, stoichiometry and oxygen content. At the same time, rare-earth ferrites provide stable magnetic and catalytic functionality with good environmental resilience. Despite having such interesting properties, depositing high-quality thin films is rather challenging and remains underexplored for rare-earth elements like Tb and Gd, because precise cation control, oxygen stoichiometry, and epitaxy are difficult and require carefully controlled growth and processing. Atomic layer deposition (ALD) could offer a solution with its self-limiting, layer-by-layer growth resulting in conformal, pinhole-free films with proper composition control. Systematic characterization using X-ray diffraction (XRD) for phase determination, X-ray fluorescence (XRF) for stoichiometry, and spectroscopic ellipsometry for optical constants and thickness will clarify structure-property relationships and processing windows. Progress in reliably depositing and characterizing rare-earth oxide perovskites like $GdNiO_3$, $TbNiO_3$, $GdFeO_3$ and $TbFeO_3$ will fill the gap and accelerate the integration of environmentally stable, multifunctional perovskite oxides into next-generation devices.

Contributed Talk 09 Thea M. Dale

Creatures in Artificial Spin Ice: emergent life-like behavior in a nanomagnetic metamaterial

Thea M. Dale[1], Arthur Penty[2], Johannes H. Jensen[2], Gunnar Tufte[2] and E. Folven[1]*

1 Dept. Electronic Systems, NTNU, Trondheim, Norway

2 Dept. Computer Science, NTNU, Trondheim, Norway

Interacting arrays of nanomagnets, known as Artificial Spin Ice (ASI), are metamaterials with rich collective behavior and promise as substrates for physical reservoir computing. Artificial life *in-materio* explores emergent life-like phenomena in physical material substrates [1]. Here, I will present our recent work in which we discover life-like "creatures" in pinwheel ASI using *flatspin* simulations combined with evolutionary algorithms. These creatures are specific domain textures in ASI that exhibit life-like behavior, such as gliders, oscillators and still lifes, inspired by cellular automata such as *Game of Life*.

A key step toward functional "artificial life" is the coexistence of multiple distinct creatures under the same conditions. In simulation, we demonstrate that gliders can coexist with stationary configurations such as still lifes, as well oscillators. In this talk, I will focus on our recent experimental realization of coexisting creatures using magnetic force microscopy (MFM) writing for state initialization. We demonstrate that a 'snake'-glider [2] and a still life can be initialized (Fig 1(a)) and driven under the same magnetic field protocol (Fig. 1(b)-(e)). Due to switching field disorder in individual nanomagnets, the state evolution in (Fig.1 (d)-(e)) deviates from ideal behavior. Nevertheless, controlled interaction is achieved, and the two states can be driven to collision (Fig. 1(f)). Our results show promise that coexistence and interaction of ASI creatures are realizable in a physical substrate, opening one pathway toward computation based on emergent dynamics in ASI.

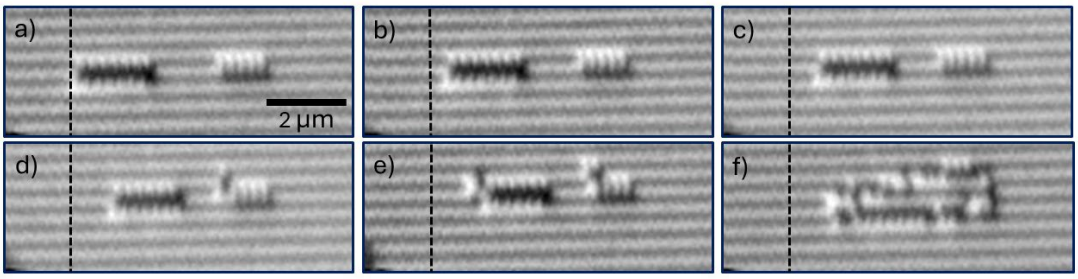

Figure 1: MFM images of a 'snake'-glider (left) moving towards a still life (right). (a) Initialization through MFM writing and external magnetic field application. (b)-(f) repeated application of external magnetic fields, moving the 'snake'-glider towards the still life, eventually leading to collision.

[1] A. Penty, J.H. Jensen, G. Tufte. Proc. of the 2025 Artificial Life Conference (2025)

[2] A. Penty, J.H. Jensen, I. Breivik et al. Nature Communications 16, 7500 (2025)

Development of in-situ bias TEM chip production with magnetic thin-films, which also allows for correlative studies of identical films

Sindre Vie Jørgensen[1],

Patrick R. B. Thomassen[1], Trond Hauklien[1], Marthe

Linnerud[1], Asle Sudbø[1], David Barriet[1,2], and Magnus Nord[1]

— 1IFY, NTNU, Norway

— 2NYB Partner DA

Through the application of various lithography and fabrication techniques, a “frontside-then-backside” method has been developed, which allows for the simultaneous fabrication of multiple In-Situ biasing TEM chips for thin film samples which are undisturbed by the process and can be created with high reproducibility and yield.

This method, depicted in Figure 1, starts with a 200 um thick, 4-inch Si wafer with 30 nm Si_3N_4 membrane on each face, and creates 100+ samples (Figure 2.1) which are highly customizable and adapted to fit a commercial in-situ TEM holder (Figure 2.2). The samples can contain multiple designs, suspended on electron transparent windows (Figure 2.3) which can have different sizes and circuitry layout with next to no variation in production time, and due to the use of EBPVD, the deposited magnetic films are very uniform with low deviation between each chip.

Using these samples, preliminary investigation of how application of a biasing current affects the movement of magnetic domain walls in 20nm thick permalloy thin films has been performed (Figure 2.4) and will be presented. Moving forwards, the method will be used to investigate how local chemistry and structure variation can affect the pinning magnetic domains.

Figure 1

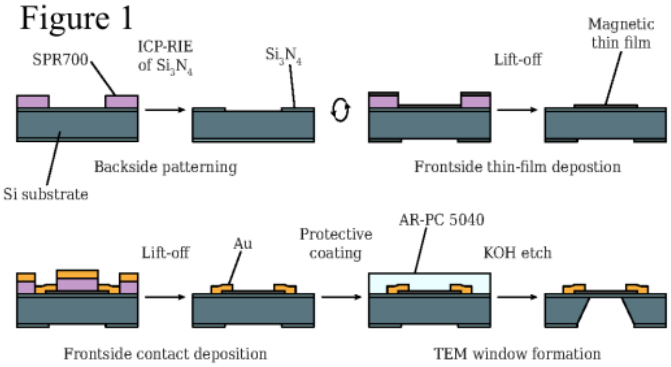

Figure 2:

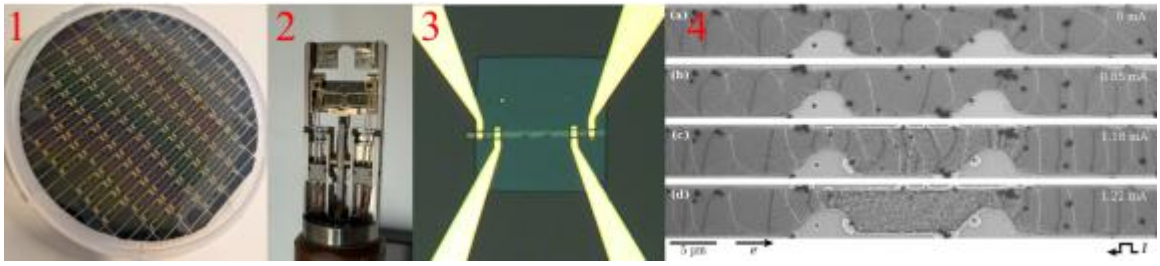

Emergent non-reciprocity and unidirectional domain dynamics in a magnetic metamaterial

Ida Breivik[1]*, Johannes H. Jensen[1], Arthur Penty[1], Anders Strømberg[1], Dheerendra S. Bhandari[1], Thea M. Dale[1], Henrik Tidemann Kaarbø[1], Michael Foerster[2], Miguel Angel Niño[2], Deepak Dagur[2], Magnus Själander[1], Gunnar Tufte[1], Erik Folven[1]

[1] Norwegian University of Science and Technology, 7030 Trondheim, Norway
[2] ALBA Synchrotron Light Facility, Carrer de la Llum 2-26, Cerdanyola del Valles, 08290, Barcelona, Spain

Artificial spin ices (ASIs) are magnetic metamaterials consisting of interacting nanomagnets. ASIs have shown promise for use as substrates for low-power, *in-materio* reservoir computing [1], but seem to lack the memory capacity of a fully functional reservoir computing device. By tailoring the geometry of the ASIs, we can change how the nanomagnets interact and tune the collective magnetic behavior of the metamaterial. To date, most ASI research has been focused on symmetric geometries. However, breaking the inversion symmetry of the system may enable a wider range of exotic metamaterial properties, such as emergent non-reciprocity. Such non-reciprocal behavior is important for enabling directional information flow, which would vastly improve the memory capacity of ASIs. Recently, we demonstrated that it is possible to break symmetry by careful initialization of magnetic domain states which can be translated unidirectionally through a symmetric ASI [2].

Here, we instead break inversion symmetry in the ASI geometry, shown in Figure 1a, resulting in a system with an inherent directionality. When subjecting the ASI to a series of in-plane, global magnetic fields, we can grow magnetic domains in a single direction, as shown in Figure 1b. In simulation, we are also able to combine growth and reversal of domains to translate the domain through our metamaterial. The unidirectional domain growth (and movement) suggests that the metamaterial exhibits an emergent non-reciprocity. This makes the system interesting as a model system for other non-reciprocal physical phenomena and could be useful in developing ASI based reservoir computing hardware.

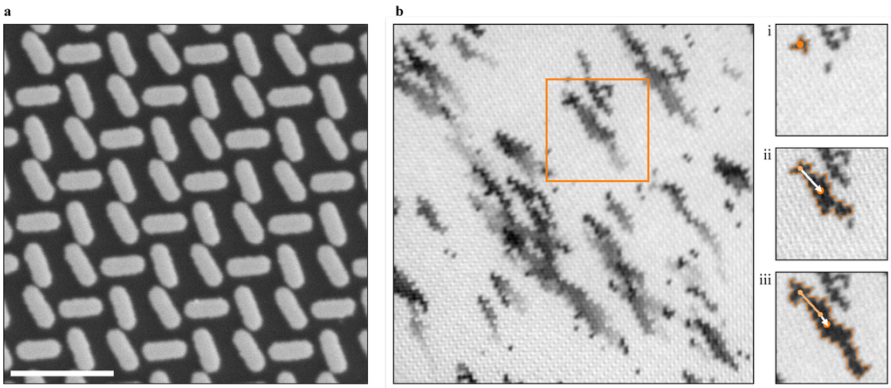

Figure 1 (a) SEM micrograph of the directional ASI. Scale bar: 500 nm. (b) Average intensity of 31 XMCD-PEEM images of the directional ASI under astroid clocking. The imaged area is 19 µm × 19 µm. We start from the white, polarized state, and grow black domains. Domains grow predominantly in the southeasterly direction, as shown by the gradient (from black to white) in the average image. (i-iii) Snapshots of the orange region of (b) at three intervals of the clocking series: after three (i), six (ii) and nine (iii) full clock cycles. The center of mass of the domain is highlighted by the orange dots in each frame, along with the previous centers of mass and arrows highlighting its movement.

[1] Jensen, J. H. & Tufte, G. Reservoir Computing in Artificial Spin Ice. in *The 2020 Conference on Artificial Life* 376–383 (MIT Press, Online, 2020). doi:10.1162/isal_a_00268.
[2] Penty, A. *et al.* Controllable gliders in a nanomagnetic metamaterial. *Nat Commun* **16**, 7500 (2025).

Seeing the invisible – upconversion of mid-infrared light to visible using molecular optomechanics in dual-resonant metasurfaces

Julia Lövgren* and Angelos Xomalis
Nanoelectronics and Photonics Group, Department of Electronic Systems,
Norwegian University of Science and Technology (NTNU),
O.S. Bragstads plass 2b, NO-7491 Trondheim
julia.lovgren@ntnu.no

Detection of mid-infrared (mid-IR) light is a key component in environmental monitoring, biomedical sensing and other applications, as this spectral region contains molecular vibrational modes. However, current state-of-the-art IR detectors remain impractical due to their sensitivity to thermal noise, demanding operation at cryogenic temperatures. This is especially problematic for device miniaturization essential for on-chip quantum applications. To tackle this issue, mid-IR photons can be "upconverted" to the visible domain, where detectors are more efficient and cost-effective [1-2].

In this work, we investigate upconversion of low energy mid-IR to high energy visible photons using a plasmonic metasurface capable of confining both visible and mid-IR light simultaneously onto a molecular monolayer on the surface. The molecular layer of biphenyl-4-thiol (BPT) is selected due to its simultaneously Raman and IR active vibrational modes, allowing nonlinear frequency mixing of IR and visible photons. The mid-IR photons are upconverted and detected as enhanced sidebands in the visible surface-enhanced Raman (SERS) spectrum. Our metasurface platform consists of slit resonators in a thin Au layer, enabling spectrally tunable polarization-dependent resonances in the mid-IR range. In addition, we employ Au nanoparticles (NPs) as antennas for visible light. The polarization sensitivity of the resonances allows our system to match dual vibrations of BPT, selecting a vibration by tuning the polarization of the incident light beams. Our structure shows promise towards simplified detection of multiple frequencies in the mid-IR regime at room temperature using miniaturized architectures.

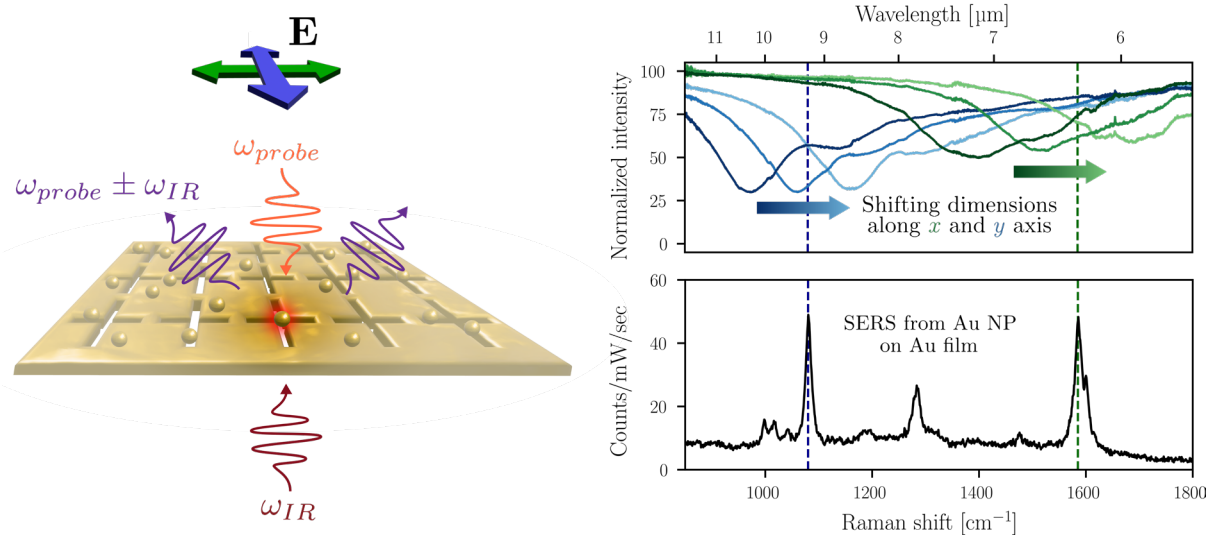

References

[1] Angelos Xomalis *et al.*, Detecting mid-infrared light by molecular frequency upconversion in dual-wavelength nanoantennas. *Science* **374**, 1268-1271 (2021). DOI:10.1126/science.abk2593

[2] Wen Chen *et al.*, Continuous-wave frequency upconversion with a molecular optomechanical nanocavity. *Science* **374**, 1264-1267 (2021). DOI:10.1126/science.abk3106

Resolving Operando Breathing of Li-ion Batteries with X-ray Computed Tomography

Shibi Tharayanmaru Palliyalil[1*], Basab Chattopadhyay[1], Steven T. Boles[2], Dag W. Breiby[1]

[1]*Dept. of Physics, Norwegian University of Science and Technology, Trondheim, Norway*
[2]*Dept. of Energy and Process Engineering, Norwegian University of Science and Technology, Trondheim, Norway*

Li-ion batteries are a significant energy carrier powering many applications today. However, they are currently plagued by many limitations such as capacity fade, cycle life, and safety concerns [1]. Therefore, it is important to investigate lithium-ion batteries with a particular focus on their safety conditions, while also emphasizing degradation studies. Gaining insight into battery safety necessitates a thorough understanding of their electrochemical operation and internal structural configuration. The present study specifically investigates cylindrical lithium-ion batteries formats, such as AAA and 18650. X-ray computed tomography (CT) is an experimental technique relevant in battery research as it is well suited for operando studies of battery processes and structural evolution [2].

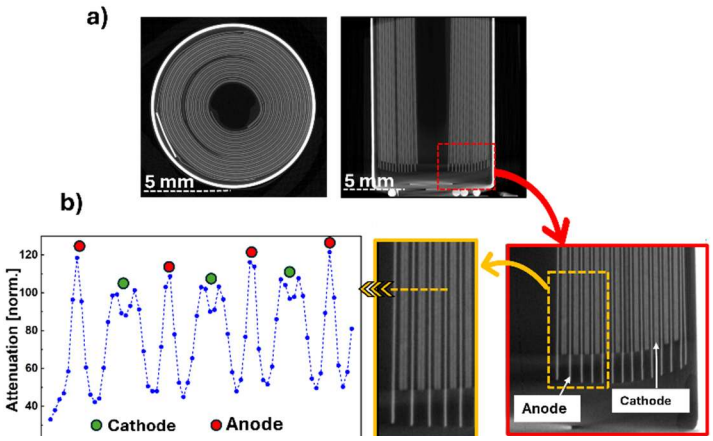

Fig 1 : Horizontal and vertical slice of a AAA battery, white dotted line indicated the position of the horizontal slice b) Magnified view of the periodic electrode arrangement. Left: intensity profiles across 1 mm of jelly roll, including 3 cathode layers and 4 anodes.

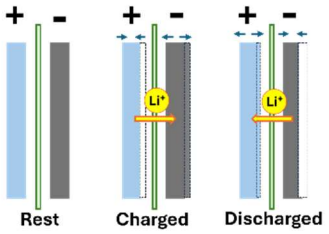

Fig 2: Electrode thickness changes during charge-discharge cycling

In this study, we investigate the structural evolution of cylindrical lithium-ion batteries during charge/discharge cycling using X-ray CT imaging. Commercial rechargeable Li-ion AAA and 18650 cells are analysed to capture differences in geometry, design, and internal architecture. In Fig. 1a) an example of horizontal and vertical slices from a CT scan of an AAA battery are shown. The focus of our study is on identifying dynamic changes in electrode thickness (Fig. 2), change in electrolyte level during cycling, including deformation and the development of defects. The line profile in Fig. 1b) demonstrates the periodic arrangement of the anodes and cathodes inside the battery. We can appreciate the changes in such arrangement as the battery is systematically charged and discharged [3]. In addition, other processes such as internal short circuits, gas generation, and structural instability are be probed during operation. These processes are closely linked to battery degradation and failure leading to unsafe conditions. By correlating observed structural changes with cycling conditions, this work aims to provide insights into the origin of performance loss and safety risks in cylindrical lithium-ion batteries.

[1] Chen, Siyan, Zhenhai Gao, and Tianjun Sun. "Safety challenges and safety measures of Li-ion batteries." Energy Science & Engineering 9.9 (2021): 1647-1672.

[2] Cogswell, Daniel A., et al. "Geometric Changes in Cylindrical Batteries as a Function of State of Charge." Journal of The Electrochemical Society 172.12 (2025): 120509**.**

[3] Dreier, Till, et al. "Exploring Image Quality Improvements in High-Speed Dual Threshold Photon-Counting Micro-CT." Journal of Nondestructive Evaluation 44.3 (2025): 108.

Peierls-induced topological Weyl semimetal in $PtBi_2$

Anders C.Mathisen[1], Stefanie S.Brinkman[1], Xin L.Tan[1], Øyvind Finnseth[1], Fabian Göhler[1], Chul-Hee Min[1], Jens Buck[2], Kai Rossnagel[2], Grisha Shipunov[3], Anna Isaeva[3], Jorge I. Facio[4], Hendrik Bentmann[1]

[1]Center for Quantum Spintronics, Department of Physics, NTNU, Norway
[2]Kiel University & DESY, Germany
[3]Institute of Physics, University of Amsterdam, The Netherlands
[4]Instituto Balseiro, National University of Cuyo, Argentina

$PtBi_2$ is attracting interest because of its exotic electronic properties, including bulk Weyl nodes, Fermi-arc surface states, and unconventional surface superconductivity. The emergence of Weyl nodes in materials is commonly attributed to accidental crossings between non-degenerate valence and conduction bands, while little emphasis has been placed on the physical mechanisms that induce Weyl physics. Recent theory indicates that reduced translational symmetry in the Peierls-distorted crystal structure of $PtBi_2$ constitutes a mechanism for the formation of Weyl nodes [1]. In this talk, we will present an investigation of the bulk electronic structure of $PtBi_2$ using soft X-ray angle-resolved photoelectron spectroscopy. Based on an analysis of the spectral weight across wide regions in momentum space, we show how the Peierls-distortion in $PtBi_2$ promotes the formation of Weyl nodes.

[1] S. Palumbo *et al.*, Interplay between inversion and translation symmetries in trigonal $PtBi_2$. Phys. Rev. B **112**, 205125 (2025)

Regulating interactions via Nanoscale Assembly for Uniform Adhesive Networks

Jun Chen, Jianying He.*

Jun Chen: Postdoctoral Fellow, Department of Structural Engineering, Norwegian University of Science and Technology, 7491 Trondheim, Norway.

Jianying He: Professor in Nanomechanics, Department of Structural Engineering, Norwegian University of Science and Technology, 7491 Trondheim, Norway. Corresponding author: jianying.he@ntnu.no.

Localized excessive hydrogen bonding in polymer–polyphenol systems often lead to heterogeneous crosslinking and poor adhesion stability, particularly in hydrogels [1]. Here, we introduce a nanoscale assembly strategy to regulate these interactions and improve network uniformity. As shown in Figure (a), by incorporating Iron (Fe)–phenolic coordination, tannic acid (TA) is transformed from molecularly dispersed state (~4 nm) into nanoscale assemblies (~255 nm). The introduction of hydrophobic units(H) also confirms the tunability of this assembly strategy. This transition redistributes interaction sites and helps reduce excessive hydrogen bonding with poly(vinyl alcohol) [2].

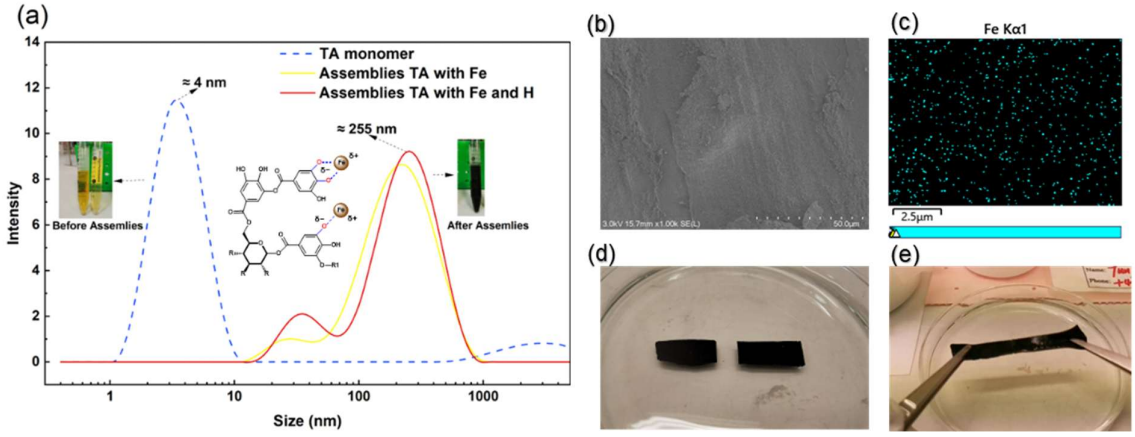

Figure 1. (a) DLS size distribution of TA before and after assembly. The blue dashed line represents TA monomers without Fe ions (PDI 0.2), while the yellow and red curves represent assembled with Fe ions and hydrophobic units (H) (PDI 0.4). The assembled TA with Fe and H was blended with poly(vinyl alcohol) to form the SEAD sample. (b) Scanning electron microscopy (SEM) image of the SEAD sample. (c) Fe elemental mapping of the SEAD sample (SEM–EDS). (d)-(e) Underwater self-healing behaviour.

To translate this assembly strategy into bulk materials, the assembled TA with Fe and H was incorporated into poly(vinyl alcohol) to obtain the SEAD sample. The SEM-EDS characterization in Figure (b)–(c) shows that iron is uniformly distributed. This confirms uniform crosslinking site distribution as Fe is located at crosslinking sites. The uniform coordination network enables dynamic bonding [3], leading to underwater self-healing (Figure (d)–(e)) through the synergy between hydrogen and coordination bonds. This work highlights nanoscale assembly as an effective strategy to regulate molecular interactions and build homogeneous networks. The resulting uniform and dynamic coordination network enable robust underwater self-healing, thereby enhancing both the functionality and reliability of the material.

References:

[1] Daiheon Lee et al., ACS Appl. Mater. Interfaces 2020, 12, 18, 20933–20941.

[2] Zhang, Z et al., Nat Commun 2025, 16, 7683.

[3] Park, H et al., Nat Commun 2023, 14, 5026.

Acknowledgment: This work is supported by the Research Council of Norway.

Contributed Talk 16 Karola Neeleman

Self-Assembling Monolayers as a Tool for Selective Chemical Solution Deposition

Karola Neeleman*, Quoc Hung Nguyen, Daniel Rettenwander, Julia Glaum, Mari-Ann Einarsrud

Department of Materials Science, NTNU Norwegian University of Science and Technology, 7034 Trondheim, Norway

A new thin-film deposition process has been developed that combines the utility of selective-area deposition and the ease of fabrication of aqueous chemical solution deposition to directly deposit microscale $BaTiO_3$ structures in a sustainable manner. Platinum substrates were successfully functionalised by patterning octadecanethiol self-assembling monolayers using DUV-photolithography, creating a hydrophobic/hydrophilic pattern on the substrate before film deposition. Altering the wetting behaviour of the substrate resulted in a high selectivity of the precursor solution for the hydrophilic regions of the substrate, allowing for precise deposition of the CSD precursor. Resolution test structures deposited with technique maintained a distinct stripe-like shape down to a feature size of 27.8 µm, and the smallest structure that was successfully deposited was as small as 15.6 µm, showing good potential as a bottom-up microscale patterning method for oxide films.

Towards reconfigurable magnonic crystals using artificial spin ice based magnetic multilayer structures

Johannes Hestmark*[1], Ida Breivik[1], Anders Strømberg[1]
Jonathan Maes[2], Jonathan Leliaert[2], Bartel Van Waeyenberge[2], Erik Folven[1]
[1]Department of Electronic systems, Norwegian University of Science and Technology, Trondheim, Norway
[2] Department of Solid State Sciences, Ghent University, Belgium

ARTIFICIAL SPIN ICES (ASIs) are metamaterials consisting of interacting, single-domain nanomagnets arranged in a wide range of geometries. As the magnetization state of these nanomagnets can be arranged into a large number of possible states, ASI systems are promising as reconfigurable magnonic crystals [1].

By coupling the ASI to a magnetic thin-film underlayer, an imprint of the ASI state onto the thin-film can be achieved, altering the propagation of spin-waves in the thin-film [2], [3]. Li et al. [3] recently show in simulation that the imprinted magnetization states in a thin-film underlayer coupled to a pinwheel ASI can be used as channels for spin waves, which can be reconfigured by manipulating the magnetic state of the pinwheel ASI.

In this work, we investigate the experimental viability of an ASI–thin-film multilayer system as a reconfigurable magnonic crystal. By engineering the dimensions of the ASI nanomagnets, we fabricate a structure designed to support spin-wave transmission along zero, one, or two preferred directions depending on the ASI magnetic configuration. We present preliminary spin-wave measurements obtained using time-resolved scanning transmission x-ray microscopy (TR-STXM), together with complementary magneto-optic Kerr effect (MOKE) microscopy images. We demonstrate spin-wave propagation in both thin-film platlets and in ASI/thin-film hybrid structures which represents an important step toward reconfigurable magnonic systems.

Preliminary TR-STXM data were obtained from both a ASI multilayer sample and a thin-film control sample. The multilayer sample consisted of a 20 nm $Ni_{0.8}Fe_{0.2}$ magnetic thin-film incorporating an artificial spin ice (ASI) structure fabricated from 20 nm $Ni_{0.8}Fe_{0.2}$, along with a 400 nm wide spin-wave antenna composed of 150 nm Cu capped with 20 nm Al. The control sample consisted solely of a 20 nm $Ni_{0.8}Fe_{0.2}$ thin-film. All structures were fabricated using electron beam lithography (EBL) lift-off.

Fig. 1(a)(i) shows a representative time slice of the TR-STXM data acquired from the control thin-film at approximately 5 GHz and zero in-plane magnetic field, where the image contrast corresponds to the out-of-plane component of the magnetization. Fig. 1(a)(ii) presents the standard deviation across all time slices after applying a Gaussian blur, highlighting the region associated with the majority of the spin-wave propagation. For comparison, Fig. 1(b) shows a MOKE microscopy image of a duplicate sample subjected to the same magnetic field protocol.

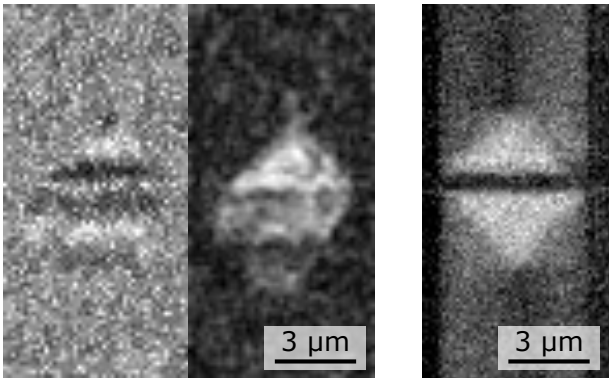

Fig. 1. (a)(i) Representative TR-STXM time slice acquired at zero in-plane magnetic field, where contrast corresponds to the out-of-plane magnetization. (a)(ii) Standard deviation of the TR-STXM signal over all time slices with a Gaussian blur, highlighting spin-wave propagation. (b) MOKE microscopy image of a duplicate 20 nm $Ni_{0.8}Fe_{0.2}$ thin-film sample showing the magnetic domain structure.

There is a clear visual correlation between the magnetic domain structure observed in the MOKE images and the spin-wave propagation pattern revealed by TR-STXM. This indicates that the thin-film domain configuration directly governs spin-wave dynamics. These preliminary results showcase that controlling the domain structure provides a viable route to tailoring spin-wave propagation. In particular, deterministic control of the thin-film domain state through the magnetic configuration of the ASI could offer a pathway toward programmable spin-wave functionality.

REFERENCES

[1] S. Gliga, E. Iacocca, and O. G. Heinonen, "Dynamics of reconfigurable artificial spin ice: Toward magnonic functional materials," *APL Materials*, vol. 8, no. 4, p. 040911, Apr. 2020. [Online]. Available: https://doi.org/10.1063/1.5142705

[2] E. Iacocca, S. Gliga, and O. G. Heinonen, "Tailoring Spin-Wave Channels in a Reconfigurable Artificial Spin Ice," *Physical Review Applied*, vol. 13, no. 4, p. 044047, Apr. 2020, publisher: American Physical Society. [Online]. Available: https://link.aps.org/doi/10.1103/PhysRevApplied.13.044047

[3] J. Li, W.-B. Xu, W.-C. Yue, Z. Yuan, T. Gao, T.-T. Wang, Z.-L. Xiao, Y.-Y. Lyu, C. Li, C. Wang, F. Ma, S. Dong, Y. Dong, H. Wang, P. Wu, W.-K. Kwok, and Y.-L. Wang, "Writable spin wave nanochannels in an artificial-spin-ice-mediated ferromagnetic thin film," *Applied Physics Letters*, vol. 120, no. 13, p. 132404, Mar. 2022. [Online]. Available: https://pubs.aip.org/apl/article/120/13/132404/2833407/Writable-spin-wave-nanochannels-in-an-artificial

Optimizing Pulsed Laser Deposition of Cr + N Co-Doped TiO_2 for Intermediate Band Solar Cells

Eskil Vik*, Joakim Christoffer Fjeld, Arne Marius Thorseth Grevskott, Magnus Sandviknes Karlsen, Morten Kildemo, Turid Reenaas

Department of Physics, NTNU

Intermediate band solar cells (IBSCs) are a solar cell concept proposed as a way to drastically increase the efficiency by which solar irradiance is converted to electric power. The key to realizing IBSCs is to develop an intermediate band (IB) material, a material with a band structure akin to a wide bandgap semiconductor, but with an additional energy band between the valence and conduction bands.

Highly Cr + N co-doped TiO_2 is proposed as an IB material, where an intermediate band would form within the intrinsic bandgap of TiO_2 from chromium 3*d* states. Nitrogen is introduced to increase the solubility of chromium in the crystal. Cr+N co-doped TiO_2 is promising due to the abundance and non-toxicity of the elements involved. However, the high levels of doping needed to form such an IB material makes growth of samples of high crystalline quality challenging.

The present reseach effort aims to enable pulsed laser deposition of highly crystalline Cr + N co-doped TiO_2 thin films. Thin films are grown to investigate the effect deposition routine, growth conditions, and substrate material have on films with varying doping levels. The crystallinity, morphology, composition and optical properties of the deposited films are characterized using techniques such as atomic force microscopy (AFM), electron microscopy, x-ray diffraction, Raman spectroscopy, and spectroscopic ellipsometry. These measurements are analysed to attain an improved understanding of the mechanisms that limit the crystalline quality as the doping level increases, and guide further efforts to achieve high quality thin films.

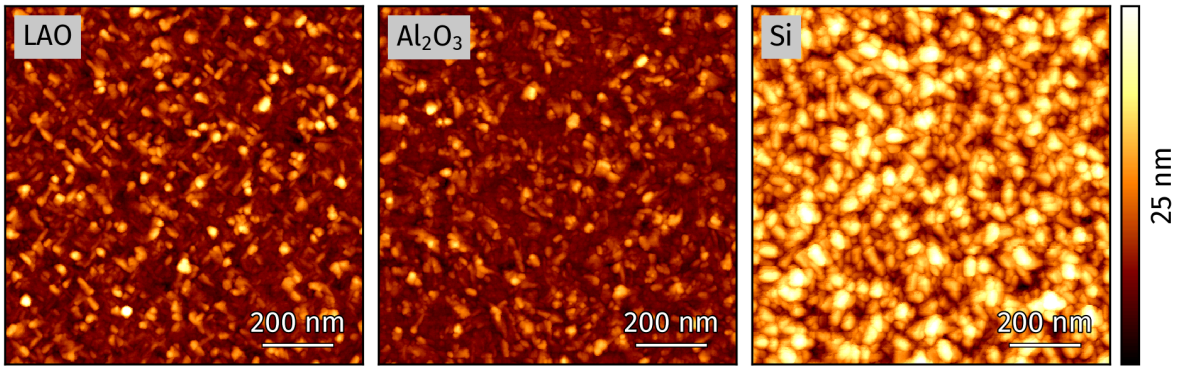

Figure 1: AFM scans of thin films grown on three substrates, illustrating the resulting differences in morphology. The film grown on Si is seen to have the highest roughness, while the film grown on LAO seems to preferentially orient grains diagonally.

POSTER-01 Jean-Claude Tinguely

Coming nanofabrication cleanroom and facilities at UiT The Arctic University of Norway

Jean-Claude Tinguely*[1], Komal Agarwal[1], Jong Wook Noh[1], Ragnar Seton[1], Olav Gaute Hellesø[1]

[1] Uit The Arctic University of Norway, Department of Physics and Technology, NO-9017 Tromsø, Norway

A new cleanroom for micro- and nanofabrication for photonics and renewable energy applications is being built at UiT the Arctic University of Norway in Tromsø with a scheduled opening in 2027. UiT's Photonics group is the main driver for the development of the laboratory. With a strong track record in integrated optics applications and optical microscopy, the new infrastructure and facilities will initially be geared towards fabrication and development of waveguides, optical components and microfluidic systems. Additionally, UiT's renewable energy research group is establishing the production of 2D materials and the Department of Geosciences will house an independent lab for high-end mass spectrometry systems (multi-collector ICP-MS/MS) in direct connection to the cleanroom. In conjunction with the new infrastructure, the Department of Physics and Technology is starting a new MSc program in Photonics and Nanotechnology which will focus on hands-on training in micro- and nanofabrication.

The clean space is distributed over close to 220 m^2, with an additional 100 m^2 prepared for expansion. The initial equipment for fabrication will include a maskless aligner, sputter coater, thermal chemical vapour deposition (CVD), furnace, plasma asher and inductively coupled plasma reactive ion etcher (ICP-RIE). For characterization, an ellipsometer, mechanical profilometer, atomic force microscope (AFM), scanning electron microscope (SEM) and confocal Raman microspectrometer will be available.

The new cleanroom is set to strengthen UiT's role as a competitive player in its fields of research, fostering impactful collaborations both nationally and internationally. UiT is a member of CC-NorChip, a collaboration between SINTEF, NTNU, UiO, USN and Electronic Coast, offering easier access to advanced technology with the aim of increasing the competitiveness of Norway's semiconductor and photonics industries.

Oblique Plane Microscopy of cardiomyoblasts from embryonic rat hearts

Hildegunn Haugan

Department of Physics and Technology (UiT), Klokkargårdsbakken 35, 9019 Tromsø
hildegunn.haugan@uit.no

The use of cell lines cardiac research has been important for the incorporation of *in vitro* models for clinical application. However, the use of *in vitro* models must be carefully translated to what happens *in vivo*. The H9c2 cell line is a widely used cell line for cardiovascular research and is derived from an embryonic rat heart. Genetically modified H9c2 cells exhibiting green (eGFP) and red (mCherry) fluorescence from intracellular mitochondria makes it possible to study the mitochondrial network within each cardiomyoblast.

OPM illuminates and images a tilted plane within the sample and can capture a three-dimensional image without having to rotate the sample. Though just recently started, I aim to use light-sheet microscopy on both a two- and three-dimensional level through OPM to analyze the morphology of cardiomyoblasts at varying cellular density and age (by passaging number). Sarcomeres and mitochondria are important for the mechanobiology of cardiomyoblasts, which makes these elements key for studies within cardiac research. The intercellular mitochondrial build-up and possible transfer will be studied based on genetically modified fluorescent labels and their localization within and outside the cells. Oblique plane microscopy (OPM) will be used for structural, morphological and organizational 3D analyses of cardiomyoblasts from rats in both fixed and live cell imaging.

Since bioimaging is the main focus of the project, an extensive and innovative use of Fiji will be implemented in order to optimize the analyses for the various samples being imaged by the microscope. Datasets will be developed, analysis methods tailored to the cells of interest and measurements performed on the individual cells' morphology in hopes of gaining further insight into the cell biology and pathology. By combining a state-of-the-art microscopic instrument with excellent cardiac *in vitro* models, advanced bioimaging may reveal pioneering data within the field of cardiac research. Figure 1 displays a network of green fluorescent cardiomyoblasts from live imaging by oblique plane microscopy.

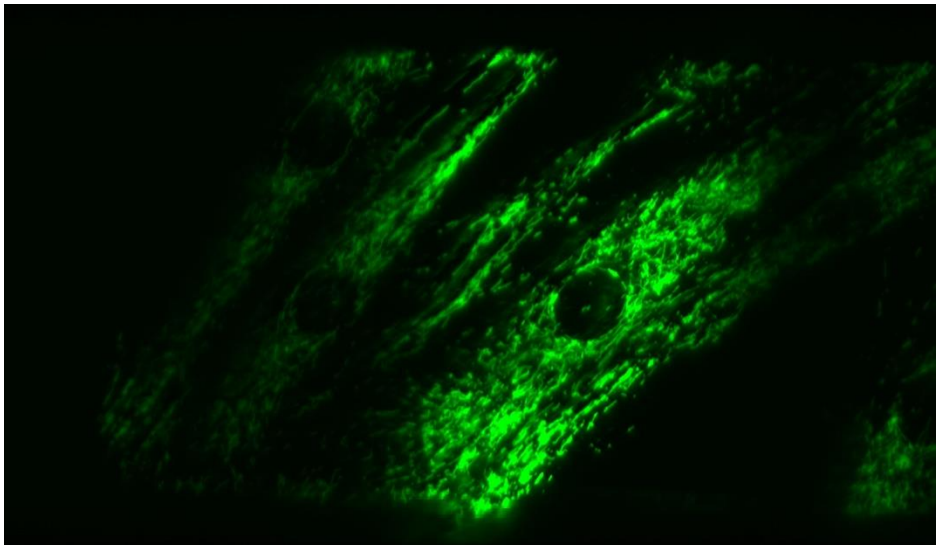

Figure 1 Post processed and deskewed image of of H9c2 cells by live imaging oblique plane microscopy displaying green fluorescent (eGFP) mitochondria in cardiomyoblasts within close proximity.

NTNU

Stability Studies of Pickering Foams with Microfluidic Techniques

April 15, 2026

Jean-Baptiste Boyssou[1]*, Maria Fernandino[2], Nadia Shardt[1]

**Presenter*

Email Addresses: JB. Boyssou (jean.b.boyssou@ntnu.no), N. Shardt (nadia.shardt@ntnu.no)

1. *Ugelstad Laboratory, Department of Chemical Engineering, Norwegian University of Science and Technology (NTNU), 7041 Trondheim, Norway*
2. *Thermal Two-Phase Flow Laboratory, Department of Energy and Process Engineering, Norwegian University of Science and Technology (NTNU), 7041 Trondheim, Norway*

Abstract

Stability of colloidal system is of paramount interest, both to enhance long term stable properties for much needed products - such as shaving cream or mayonnaise - and to induce destabilization and consecutive disappearance of undesired phases - such as metallic foam in aluminum smelting.
Among possible stabilizing reagents for colloidal systems, nanoparticles (NPs) have gained traction over the past years, due to their dual properties through optical or magnetic activity, as well as their large biocompatiblity and chemical inertia. Emulsions stabilized with nanoparticles are named Pickering emulsions, after the pioneering work of P. Pickering in 1907.
Pickering foams, composed of gas-liquid mixtures stabilized by the presence of nanoparticles, are believed to be stabilized by two main mechanisms: the drastic reduction of Ostwald ripening rates and the large steric hindrance between armored bubbles, both due to the adsorption of NPs at the surface of the gas phase. NPs will adsorb in an irreversible way at the surface of the gas bubbles, with a typical energy of desorption of a few $k_B T$. As a result, Pickering foams are believed to be very stable compared with surfactant counterparts, in which constant absorption/desorption of the surfactant is taking place.
In order to assess the stability of such systems at the level of individual bubbles, microfluidics appears to be of great potential. Leveraging the fine control over bubble size during generation, as well as discrete phase flow rates and confinement, image-based assessment of the foam stability can be conducted.
In this study, we considered presence of titanium dioxide TiO_2 nanoparticles to stabilize bubbles in a continuous media composed of acrylate and additional species in view of photopolymerization of the resulting Pickering foam to create porous materials.
The coalescence frequency, bubble size and dispersity as well as foam height and volume fraction are measured over time from optical microscopy imaging, both on a microfluidic platform and in the bulk. Additional comparison of these microfluidic-generated foams is being done with Pickering foam resulting from incorporation of air with an emulsion-maker. The study of stabilize at the bubble-bubble level thanks to microfluidics can help understanding stability of Pickering foams at the macroscale, which can be leveraged to actively enhance or reduce stability of desired system.

Inverse design of nanomagnet shape for tailored angle-dependence of magnetic switching

Henrik T. Kaarbø[1], and Erik Folven[1]
[1] Department of electronics, Norwegian University of Science and Technology (NTNU), Trondheim, Norway

Patterned 2D nanomagnets comprise a broad range of complex, interacting many-body systems subject to extensive study within the field of magnetics, as well as the broader fields of condensed matter physics and informatics. At the nano- to mesoscale, the equilibrium magnetization of a given domain is determined by a non-linear competition between exchange and demagnetization energies; their relative strength is tunable by engineering the domain's shape. This in turn allows for the realization of magnetic metamaterials with rich and tunable physics. However, when simplifying assumptions like coherent rotation fail, the nonlinear interactions renders the task of predicting the magnet shape corresponding to the desired energetics a problem that requires special insight, paired with resource consuming experiments and/or manually defined and computationally intensive simulation sweeps. In this study, we aim to demonstrate that the shape of the nanomagnet corresponding to a target switching curve can be found automatically by solving an inverse problem computationally with NeuralMag, using minimal knowledge of the target shape's magnetization dynamics. Simultaneously, we showcase the applicability of recently enabled scientific machine learning approaches in micromagnetics.

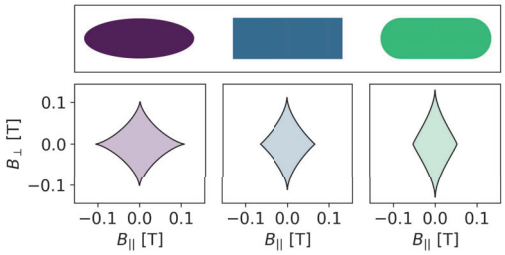

(a) **Above**: Common geometries for nanomagnets used and studied in the Artificial Spin Ice literature, from dark to light: ellipse, square and stadium shapes. **Below**: correspondingly colored micromagnetically simulated switching curves for $220\,\mathrm{nm} \times 80\,\mathrm{nm} \times 10\,\mathrm{nm}$ magnets with these shapes.

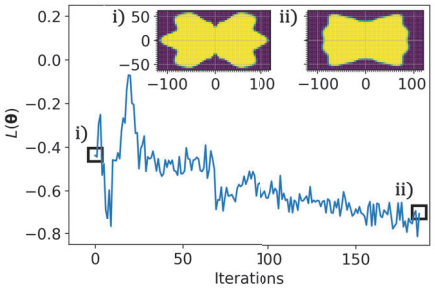

(b) $L(\boldsymbol{\theta})$ evaluated over the run shown in Fig. 3, targeting a $220\,\mathrm{nm} \times 100\,\mathrm{nm} \times 10\,\mathrm{nm}$ stadium shape's switching curve. **i)-ii)** Initial and final magnet shape and their respective evaluation of $L(\boldsymbol{\theta})$ inside boxed markings. The nanomagnet's extent is given in nanometers.

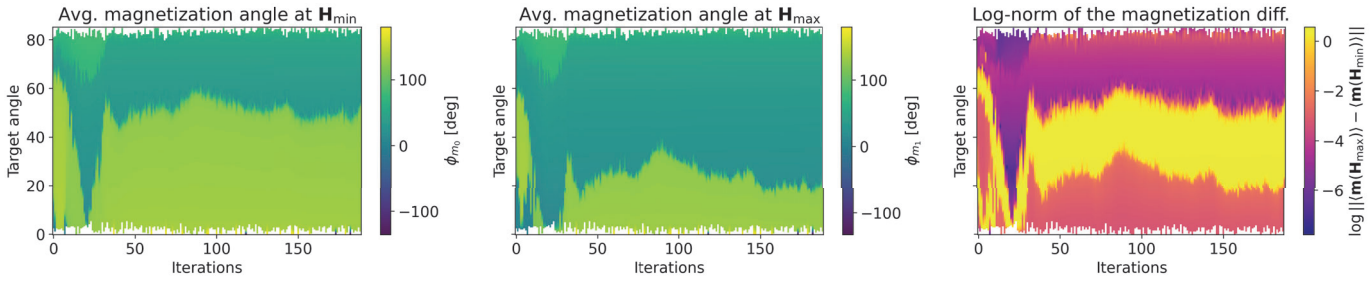

Fig. 3: Compliance with target switching curve at a given angle ϕ over number of iterations of gradient descent upon the parametrized nanomagnet shape. **Left**: average magnetization angle when $\boldsymbol{H}_{\mathrm{ext}} = \boldsymbol{H}_{\min}(\phi)$. An angle close to the initial magnetization angle at 180 degrees is desired. **Middle**: average magnetization angle when $\boldsymbol{H}_{\mathrm{ext}} = \boldsymbol{H}_{\max}(\phi)$. A magnetization angle close to a reversed magnetization at 0 degrees is desirable. **Right**: The log-norm of the difference between the spatial average of the magnetization, denoted by $\langle \boldsymbol{m} \rangle$, at $H_{\min}(\phi)$ and $H_{\min}(\phi)$. A difference close to unity is desirable, as it indicates magnetization reversal has occured within the interval $[\boldsymbol{H}_{\min}(\phi), \boldsymbol{H}_{\max}(\phi)]$.

Alginate-encapsulated bone spheroids: approaches to study bone cells in 3D

D. Boscaro*[1], S. Kjeldgaard-Nintemann[2], A. Bjørkøy[1], P. Sikorski[1]

[1]*Department of Physics, Norwegian University of Science and Technology, NTNU, Norway*

[2]*Center for Advanced Bioimaging, Department of Plant and Environmental Sciences, University of Copenhagen, Copenhagen, Denmark*

INTRODUCTION: Spheroids with their extensive cell-cell and cell-extracellular matrix (ECM) interactions [1], are considered a suitable model for investigating bone ECM and bone mineralization process in vitro. Bone ECM is composed of an inorganic and organic part, made up mostly of carbonate-substituted calcium-deficient apatite (Calcium Phosphate, CaP) and type I collagen respectively [2]. Adequate characterization techniques and proper optimization of the already existent methods are required to study these 3-dimensional cell models and the characteristics of the produced mineral.

METHODS: MC3T3-E1 spheroids were obtained using the micro-mold [3] technique and were subsequently embedded in an alginate hydrogel. To evaluate ECM deposition and mineralization, Second Harmonic Imaging Microscopy (SHIM) and Coherent Raman Scattering microscopy (CRS) were used. Transmission Electron Microscopy (TEM) was also performed to provide additional support to the observed data.

RESULTS: Alginate-encapsulated spheroids were followed in culture for up to 4 weeks. SHIM revealed the presence of collagenous matrix in differentiation media (OM) cultured spheroids starting from week 2 (Fig. 1). CRS performed on intact spheroids cultured for 4 weeks showed the presence of phosphate positive regions, detected also in the core region of the aggregate (Fig. 2A). CRS was also performed to observe the localization of the cells and the deposited matrix (Fig. 2B). TEM images (Fig. 3) supported the results observed with SHIM and CRS.

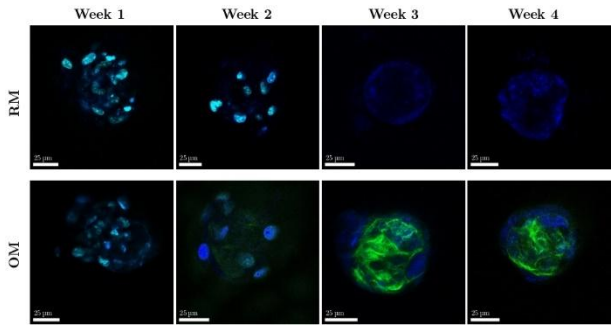

Fig. 1: SHIM of regular and differentiation media cultured spheroids. A progressive increase in collagen production (green) can be observed from week 2 to 4 in OM cultured spheroids.

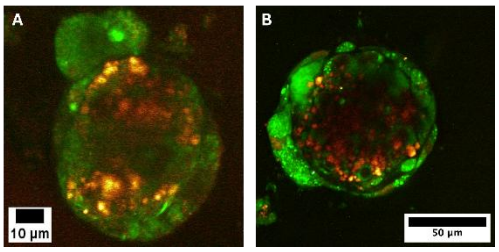

Fig. 2: A) CRS and Second Harmonic Generation microscopy performed on spheroids to detect the deposited ECM (collagen in green and phosphate-positive regions in red). B) CRS was performed to localize the cells (green) and the mineralized deposits (red).

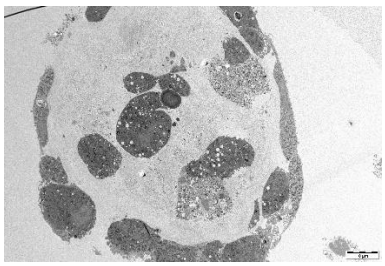

Fig. 3: TEM image of a representative spheroid cultured for 6 weeks in OM

DISCUSSION & CONCLUSIONS: The results show that alginate-encapsulated spheroids can be a suitable model for studying bone ECM deposition and mineralization. SHIM and CRS were observed to be two suitable models to perform label-free imaging of intact, embedded spheroids.

REFERENCES: [1] S. J. Kim et al (2020) Advanced Healthcare Materials, 9.23: 2000608; [2] Mansour et al (2017), Tissue Engineering part A 23.23-24: 1436-1451; [3] A.P. Napolitano et al (2007) Biotechniques, 43.4:494-500.

ACKNOWLEDGEMENTS: This project was founded by the Norwegian University of Science and Technology (NTNU). We acknowledge Stiftelsen Biopolymer for additional financial support. We acknowledge BNMI for the financial support. We acknowledge Nan Tostrup Skogaker for training, technical assistance and access to the electron microscopy core facility, NTNU.

POSTER-06 Saber Mohammadi

An Operational Flow Assurance Approach to Asphaltene and Wax Control Using Single-Walled Carbon Nanotubes: Experimental Field-Condition Study

Saber Mohammadi[1], Fatemeh Mahmoudi Alemi[2]

[1] *Department of Geosciences, Norwegian University of Science and Technology (NTNU), Trondheim, Norway*

[2] *Petroleum Engineering Department, Research Institute of Petroleum Industry (RIPI), Tehran, Iran*

Abstract

Organic deposition by asphaltenes and wax remains one of the most persistent flow assurance risks across the production system, from the near-wellbore region to tubing, flowlines, and surface handling facilities. In practice, these two deposition mechanisms are commonly treated with separate chemicals, which increases operating cost, chemical compatibility risk, and treatment complexity. This study presents an operational flow assurance approach based on single-walled carbon nanotubes (SWCNTs) for the simultaneous control of asphaltene and wax under representative field conditions. The work was carried out on live and dead crude oil samples using high-pressure/high-temperature experimental methods designed to reflect actual production environments. For the asphaltene side, solid detection system and high-pressure microscopy tests showed that SWCNT treatment shifted the asphaltene onset pressure from 5946 psi to 4375 psi at 125 °C, indicating a wider operational window before solid precipitation begins. In parallel, the nanotubes significantly reduced asphaltene aggregate growth during depressurization, confirming their dual role as both inhibitor and dispersant under field-relevant conditions. The effect is attributed to strong intermolecular interaction between SWCNT surfaces and asphaltene molecules, which improves colloidal stability and limits particle growth. For wax control, cross-polarized microscopy, DSC, and rheological measurements demonstrated an optimum SWCNT dosage of 75 ppm. At this concentration, the wax appearance temperature was reduced from 32.6 to 23.2 °C and the gelation point from 21.5 to 14.7 °C. In addition, wax crystal morphology shifted from dense spherical-like structures to finer needle-like crystals, while average crystal size decreased from 756 to 86 nm. These changes translated into improved crude oil mobility and lower viscosity below WAT, supporting the potential of SWCNTs as an integrated flow improver for waxy systems. Overall, the results indicate that low-dose SWCNTs can provide a single-chemical strategy for simultaneous mitigation of asphaltene and wax risks, with potential benefits in production continuity, chemical program simplification, and reduced intervention frequency. The findings support the applicability of SWCNT-based treatment as a practical flow assurance option for field operations where both organic deposition mechanisms must be managed together.

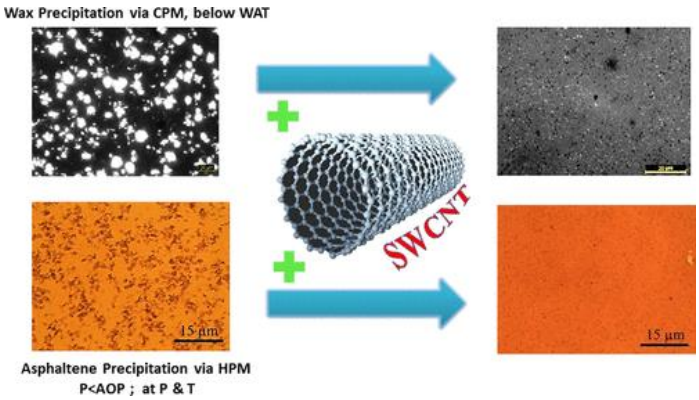

POSTER-07 Mina Alexandra Thor

Second- and third-order nonlinear optical processes in III–Phosphide phonic integrated platforms.

Author Mina Alexandra Thor

Supervisor Prof. Johann Riemensberger, Co- supervisor Prof. Astrid Aksnes

Affiliation NTNU

Second- and third-order nonlinear optical processes (χ^2 and χ^3) in III–V photonic platforms enable compact and efficient optical parametric amplification (OPA) and oscillation (OPO) for integrated photonics. III–V materials such as InGaP and GaP are particularly attractive due to their large nonlinear coefficients, high refractive index, and wide transparency windows, supporting both χ^2-driven parametric gain and Kerr (χ^3) frequency conversion on-chip . While Kerr OPO relies on four-wave mixing in χ^3 media to generate signal and idler waves over broad spectral ranges, χ^2-based OPA offers higher efficiency and lower threshold through three-wave mixing processes.

In (In)GaP, the coexistence of strong χ^2 and χ^3 nonlinearities enables hybrid parametric platforms combining frequency conversion and comb generation. Efficient operation requires phase matching, which in isotropic III–Phosphied materials is typically achieved through dispersion engineering rather than birefringence. In particular, type II phase matching has been demonstrated in InGaP waveguides by engineering modal indices such that $2k_{\mathrm{pump}} = k_{\mathrm{signal}} + k_{\mathrm{idler}}$. This enables processes such as second-harmonic generation and parametric amplification between TE and TM modes.

Fabrication of these devices relies on advanced nanophotonic processing, including dry and wet etching of III–V materials. GaP-based structures, often used as a platform or template, require anisotropic etching to achieve smooth sidewalls and precise geometries critical for phase matching and low-loss propagation . Recent work demonstrates wafer-scale InGaP-on-insulator platforms with low propagation loss and high nonlinear efficiency, enabling scalable integrated nonlinear photonics.

These advances position III–V χ^2/χ^3 platforms as key enablers for quantum light sources, frequency combs, and tunable coherent light generation across visible and telecom wavelengths.

[1] M. L. Vincetti *et al.*, “InGaP χ^2 integrated photonics platform for nonlinear optics,” *Light: Science & Applications*, vol. 13, 2024.

[2] A. S. Rao *et al.*, “Wafer-scale InGaP-on-insulator nonlinear photonics platform,” *arXiv preprint*, arXiv:2406.18788, 2024.

[3] J. Leo *et al.*, “Interplay of χ^2 and χ^3 effects in microcomb generation,” *J. Eur. Opt. Soc.-Rapid Publ.*, vol. 21, no. 1, 2025.

[4] H. Jung *et al.*, “Gallium phosphide nanophotonics for Kerr frequency combs,” *ACS Photonics*, vol. 11, 2024.

[5] X. Ji *et al.*, “Ultra-efficient Kerr parametric oscillation in integrated photonics,” *Nat. Commun.*, vol. 13, 2022.

[6] A. C. Lin, “Gallium phosphide nanophotonic device fabrication and etching techniques,” Ph.D. dissertation, Stanford University, Stanford, CA, USA, 2023.

[7] J. S. Pelc *et al.*, “Integrated nonlinear photonics in III–V semiconductors,” *Light: Science & Applications*, vol. 13, 2024.

[8] D. Grassani *et al.*, “Microwave-to-optical frequency conversion and nonlinear processes in InGaP waveguides,” *Optica*, vol. 7, no. 6, pp. 731–737, 2020.

[9] C. Reimer *et al.*, “High-efficiency frequency conversion in integrated nonlinear platforms,” *Optics Express*, vol. 27, no. 5, pp. 6535–6546, 2019.

[10] M. Pu *et al.*, “Efficient frequency comb generation in χ^2/χ^3 nonlinear platforms,” *Laser & Photonics Reviews*, vol. 14, no. 8, 2020.

From Microbattery Design Strategies to Future Modelling of Novel Electrode Architectures in Lithium-Ion Batteries

Authors

Nadiia Piiter*, Iván Fernández Valencia, Eirik Odinsen, Jacob Joseph Lamb

***Presenter**

Affilation
Department of Energy and Process Engineering, Norwegian University of Science and Technology (NTNU), Trondheim, Norway

Abstract

The demand for compact, high-performance lithium-ion batteries continues to grow with the rapid expansion of miniaturised electronics, sensors, and integrated energy systems. This poster presents a review of recent advances in micro-battery design, with particular focus on microfabrication methods, nanostructured materials, 3D electrode architectures, porosity-engineered electrodes, and reduction of non-active components such as separators and current collectors. The reviewed literature shows that these design strategies can improve ion transport, active material utilisation, rate capability, and volumetric energy density, but their broader implementation remains constrained by challenges related to scalability, mechanical robustness, interfacial stability, and manufacturing reproducibility.

A central conclusion of the review is that electrode architecture is becoming as important as material chemistry in determining battery performance. In particular, gradient porosity, structured thick electrodes, and lightweight or wire-based current collector concepts appear promising for reducing transport limitations and improving high-rate behaviour, although most studies remain at laboratory scale and require stronger validation in practical cell formats.

Future work will therefore focus on physics-based and data-driven modelling of novel electrode architectures. Planned directions include proof-of-concept modelling of cathode microstructure, comparison of wire-based and foil-based current collectors, and evaluation of how structural modifications influence electrochemical, thermal, and mechanical behaviour. These studies will use computational battery models to support design optimisation and to identify electrode configurations with improved performance and sustainability potential.

POSTER-09 Na Wang

TiO_2/Co_3O_4 Heterojunction Kinetics for Betavoltaic Power Batteries

Na Wang, Kaiying Wang

Department of Microsystems, University of South-Eastern Norway, Horten 3184, Norway

This work proposes a TiO_2/Co_3O_4 heterojunction nano architectured transducer for betavoltaic power batteries and establishes a coupled Monte Carlo method-transport modeling framework. For a ^{63}Ni β source (mean energy 17.4 keV), Monte Carlo method provides layer-resolved β transport and energy deposition in the Co_3O_4 sensitization layer and TiO_2 nanotube layer, which are mapped to electron-hole pair generation and drift-diffusion collection models. Simulations show that most β energy is deposited in TiO_2, while the TiO_2/Co_3O_4 built-in field aids interfacial charge separation. An optimized geometry (TiO_2 nanotube length 3 μm; Co_3O_4 thickness 40 nm) achieves a maximum deposition efficiency of 76.3%, with mean deposited energies of 12.82 keV (TiO_2) and 0.46 keV (Co_3O_4) per β particle. The corresponding G_{ehp} is ~ 4.58×10^{21} $m^{-3}\cdot s^{-1}$ (TiO_2) and 1.38×10^{22} $m^{-3}\cdot s^{-1}$ (Co_3O_4), and the estimated collection efficiency is ~ 6.25%. Parameter sweeps quantify how geometry tunes deposition and collection, providing design guidance for high-efficiency betavoltaic transducers.

POSTER-10 Anniken Mathea Sjødal

Microbubble- and ultrasound-mediated delivery of viral vectors across the blood-brain barrier

Anniken Mathea Sjødal[*1,2], *Sigrid Berg*[3], *Rajeevkumar Raveendran Nair*[4], *Clifford Kentros*[4], *Catharina de Lange Davies*[1], *Sofie Snipstad*[1,2,5]

1. Department of Physics, Norwegian University of Science and Technology, Trondheim, Norway
2. The Neurology Department, St. Olav's Hospital, Trondheim University Hospital, Norway
3. Department of Health Research, SINTEF Digital, Trondheim, Norway
4. Kavli Institute for Systems Neuroscience, Norwegian University of Science and Technology, Trondheim, Norway
5. Cancer Clinic, St. Olav's Hospital, Trondheim University Hospital, Norway

Objectives

The aim was to deliver adeno-associated viruses (AVVs) across the blood-brain barrier in mice, enabling non-invasive gene therapy of neurodegenerative disorders such as Alzheimer's disease.

Methods

MRI-guided focused ultrasound combined with microbubbles (SonoVue) were used to open the blood-brain barrier (BBB) and deliver recombinant AAVs to one brain hemisphere in Cre reporter tdTomato mice. The intensity of a gadolinium-based contrast agent (Omniscan) was used to determine the degree of BBB opening based on T1 MR images. Whole brain optical imaging was performed to evaluate tdTomato fluorescence in sonicated areas, and confocal microscopy was employed to assess the microdistribution of tdTomato fluorescence.

Results

T1 MR images showed clear BBB opening when comparing the gadolinium signal intensity of treated and non-treated hemispheres. TdTomato fluorescence was verified in Cre reporter tdTomato mice, confirming successful Cre-AAV transduction. In general, higher AAV dosages resulted in stronger fluorescent signals. The delivery of AAVs was more efficient in the sonicated compared to the non-sonicated brain hemisphere, suggesting that focused ultrasound and microbubbles enhanced AAV uptake by increasing the BBB permeability.

Conclusions

MRI-guided focused ultrasound and microbubbles resulted in increased transduction efficiency in the sonicated brain hemisphere, demonstrating the potential of this approach for targeted gene delivery across the BBB. Future work will build on these findings by precisely delivering viral vectors to the entorhinal cortex to target specific entorhinal neuronal subtypes.

Growth Optimization of $La_{0.7}Sr_{0.3}MnO_3$ Thin Films on $LiNbO_3$ Substrate by Pulsed Laser Deposition

Payel Chatterjee[1*], Travis Edward Gustafson[1], Barbara Pacáková[1], Marius Holen[1], Johann Riemensberger[2], Erik Wahlström[1]

[1]Center for Quantum Spintronics (QuSpin), Department of Physics, Faculty of Natural Sciences, NTNU
[2]Department of Electronic Systems, Faculty of Information Technology and Electrical Engineering, NTNU

$La_{0.7}Sr_{0.3}MnO_3$ (LSMO) is a low-damping ferromagnetic perovskite widely used in magnonic systems, where control of magnon–phonon interactions is essential for emerging concepts such as bosonic information processing. Integrating LSMO with piezoelectric substrates such as $LiNbO_3$ (LNO) provides a potential route to engineer phonon–magnon coupling but achieving uniform crystalline LSMO thin film growth on LNO remains challenging due to lattice mismatch and substrate surface wetting issues.

In this work, LSMO thin films were deposited on 128° Y-cut LNO substrates using pulsed laser deposition, while systematically varying the substrate temperature (500-800°C) and oxygen partial pressure (0.1-0.2 mbar). Among the investigated growth conditions, films grown at 700°C substrate and 0.1 mbar O_2 partial pressure exhibit the best crystal quality and surface roughness. X-ray diffraction shows LSMO(110) and LSMO(220) peaks at $2\theta \approx 32.4°$ and 67.9°, respectively, corresponding to pseudocubic lattice parameters of ~3.89–3.90 Å. The comparatively enhanced LSMO(220) intensity is consistent with a textured growth exhibiting a preferred orientation. This orientation is stabilized by the symmetry of the substrate surface. The in-plane diagonal of LSMO(110) (~5.52 Å) plane is closer to the in-plane periodicities of 128° Y-cut $LiNbO_3$ (~5.15 Å), resulting in a reduced lattice mismatch (~7%). The atomic force microscopy image shows a granular surface morphology with a root mean square (r.m.s) roughness of ~2.8 nm for these films. Magnetic measurements (M–T) show a ferromagnetic transition with a Curie temperature around 330 K.

These results demonstrate the feasibility of LSMO growth on $LiNbO_3$; however, further optimization is required to reduce surface roughness and grow epitaxial monolayers. This is essential for systematic strain engineering and interface-driven phonon–magnon coupling in oxide heterostructures.

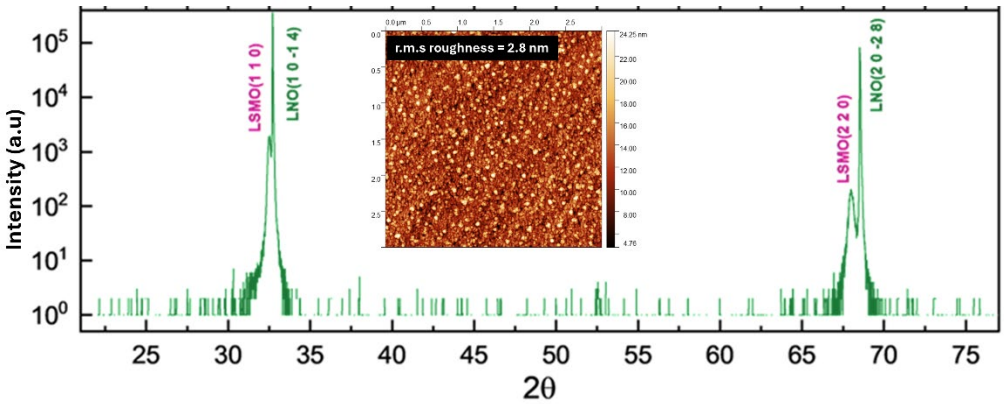

Figure 1: XRD pattern shows LSMO(110) and LSMO(220) peaks along with substrate peaks. Inset: AFM image showing the granular surface morphology of the film with r.m.s roughness of 2.8 nm.

POSTER-12 Ece Kurt Majidli

Integration of Carbon Nanotubes for Nanoelectronic Devices and Sensing Applications

Ece Kurt Majidli[*], Avisek Roy[1], Knut Eilif Aasmundtveit[1], Henning Gundersen[2], Steven Bos[2]

[*,1]Department of Microsystems, Faculty of Technology, Natural Sciences and Maritime Sciences, University of South-Eastern Norway, Campus Vestfold, Norway

[2] Department of Science and Industry systems, Faculty of Technology, Natural Sciences and Maritime Sciences, University of South-Eastern Norway, Campus Kongsberg, Norway

Abstract:

As transistor dimensions shrink below about 10 nm, conventional planar silicon CMOS technologies encounter fundamental scaling limits. Therefore, nanomaterial-based approaches are increasingly gaining attention in future compact, low-power, and highly sensitive sensing and computing systems. Carbon nanotubes (CNTs) are particularly promising due to their superior electrical properties, 1-D structures and diverse applications in both sensing and transistor technologies.

This PhD project focuses on developing and evaluating two complementary CNT integration strategies for future computing and advanced sensing applications. The first direction investigates localized on-chip CNT growth for integrated sensing applications. Direct CNT integration on CMOS chips could enable compact, wireless, power-efficient and low-cost smart sensors, in which CNTs serve as the sensing material while signal processing is carried out on-chip by CMOS circuitry. This part of the project aims to optimize localized low-temperature CNT growth using different catalyst materials while achieving high growth density, controlled CNT morphology, low defect levels and compatibility with scalable wafer-level fabrication.

The project also explores the development of CNT-based field-effect transistors (CNTFETs) for ternary computing. Semiconducting CNTs are attractive transistor channel materials because of their one-dimensional structure, high carrier mobility and diameter-dependent electronic properties. In particular, this work aims to achieve threshold-voltage tuning for multi-valued logic (MVL) design through the selective integration of semiconducting CNTs with different diameters.

This PhD research integrates materials processing, device fabrication and characterization to contribute to the future of integrated circuit (IC) fabrication and digital system design. The poster will provide an overview of the overall research roadmap, planned fabrication strategies and the experimental direction of the project at the University of South-Eastern Norway.

Keywords: Carbon nanotubes (CNTs), carbon nanotube field-effect transistor CNTFET, CMOS, integrated circuit (IC), ternary computing, multi-valued logic (MVL), smart sensors.

POSTER-13 Ali Pourabdollah Vardin

Next-Generation Mobile Micro-IDT Acoustic Generators for Biological Applications

Ali Pourabdollah Vardin[1, *], Hyunjin Yong[2], II Woong Park[2], Maria Fernandino[1], and Carlos A. Dorao[1]

[1]Department of Energy and Process Engineering, Norwegian University of Science and Technology, Trondheim, Norway

[2]Inha University, South Korea, Inha-ro 100, Incheon, Republic of Korea

Introduction:

Surface Acoustic Waves (SAW) have provided remarkable capabilities for micro- and nanosize particle manipulation. Most acoustofluidic devices are based on a milimeter-size interdigitated transducer (IDT) placed close to a microliter droplet for microchannels containing the sample, see Fig 1.A. Such concepts are not compatible with common labware such as standard well plates or centrifuge tubes requiring processing of larger sample volumes. In this work, we show the development of a new acoustofluidic concept based on mobile-micro-size acoustic generators resembling a needle, Fig. 1.B. The potential of this new concept applied for the extraction of the DNA from HEK293A cells.

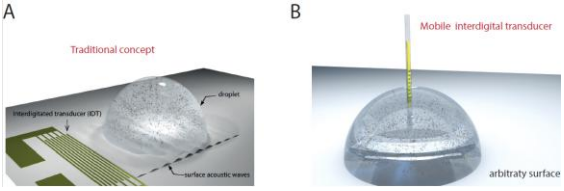

Figure 1. Schematics of **(A)** traditional stationary SAW architecture and **(B)** our mobile micro-IDT platform.

Microfabrication of the mobile interdigital transducer:

The mobile generators were fabricated on 128° Y-X lithium niobate wafers using a standard lift-off process. The process, detailed in Figure 2, allows for high-throughput production of over 100 devices per wafer.

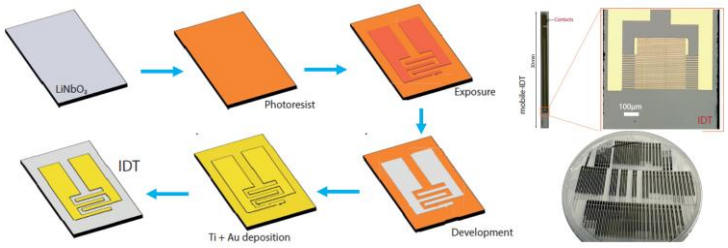

Figure 2. Fabrication workflow, device dimensions, and real images of the micro-IDT.

Streaming Visualization and Cell Lysis Performance:

Performance was validated via Particle Image Velocimetry (PIV) to characterize the acoustic streaming. As shown in Figure 3A, high-velocity streamlines at the micro-aperture generate the shear forces necessary for cell lysis. Figure 3B displays the DNA content measured after lysis, demonstrating results comparable to conventional chemical methods within seconds and without reagents.

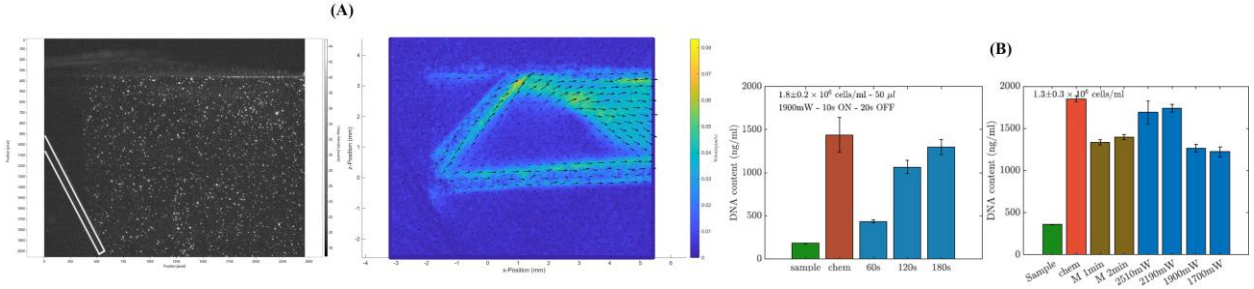

Figure 3. (A) PIV flow field at the micro-aperture and (B) DNA content after lysis compared to chemical methods.

Conclusion:

We developed a mobile IDT platform for efficient cell lysis within standard tubes. The miniaturized design reduces costs by minimizing substrate usage and cleanroom requirements. This architecture provides a flexible, cost-effective alternative to stationary SAW devices, enabling rapid HEK293A lysis in arbitrary containers.

POSTER-14 Guoli Zhang

Boosting Zinc-Ion Hybrid Capacitors with Mesoporous Carbon Derived from Highly Graphitized Carbon Quantum Dots

Guoli Zhang and Kaiying Wang

Department of Microsystems, University of South-Eastern Norway, Horten 3184, Norway

The high mesopore fraction and excellent electrical conductivity of porous carbon significantly enhance the energy and power densities of zinc-ion hybrid capacitors (ZIHCs). However, conventional activation methods often fail to achieve a high mesopore ratio while maintaining structural integrity and conductivity. This study presents an innovative strategy that utilizes highly graphitized nitrogen-doped carbon quantum dots (NCQDs) as precursors to fabricate mesoporous carbons (MCs) with an ultra-high specific surface area, a dominant mesopore fraction, and superior conductivity. Coal tar pitch (CTP) is pretreated using a deep eutectic solvent (DES) to extract an aromatic-rich fraction (DCTP), which is then converted into graphitized NCQDs. Subsequent KOH activation of these NCQDs constructs a well-developed hierarchical porous network. The optimized material, M-MCs, achieves an impressive specific surface area of 3328 $m^2\ g^{-1}$ and a mesopore content of 83.3%, enabling rapid Zn^{2+} storage kinetics. As a ZIHC cathode, M-MCs deliver a remarkable specific capacity of 272.8 mAh g^{-1} at 0.1 A g^{-1}, a high energy density of 218.24 Wh kg^{-1}, and a power density of 15.96 kW kg^{-1}, while maintaining 94% capacity retention after 8,000 cycles at 5 A g^{-1}. Even at an ultra-high current density of 20 A g^{-1}, a capacity of 116.4 mAh g^{-1} is retained. This strategy provides a promising avenue for the development of high-rate carbon cathodes, paving the way for next-generation energy storage and wearable electronics.

Innovative GeSi wall waveguides for on-chip broadband mid-IR spectroscopy

Noémie Mestre[1*], Martin Feiler[1], Nooman El Bouchikhi[2], Victor Turpaud[2], Giovanni Isella[3], Jacopo Frigero[3], Delphine Marris-Morini[2], Jana Jágerská[1]
[1]The Arctic University of Norway (UiT), Klokkargårdsbakken 35, NO-9037 Tromsø
[2]Centre de Nanosciences et de Nanotechnoligies (C2N), 10 Bd Thomas Gobert, FR-91120 Palaiseau
[3]L-NESS, Politecnico di Milano Dipartimento di Fisica, I – 22100 Como, Italy
noemie.mestre@uit.no

Absorption spectroscopy is a powerful tool to tackle societal challenges in areas such as environmental monitoring and health care, as it offers high gas specificity, low measurements drift, and allows in situ non-destructive measurements with low limits of detection. The miniaturization using integrated optics is an important step towards scalability and portability; however, it remains challenging as it requires long, complex, and specially tailored nanophotonic structures. Until recently, integrated sensors were often limited by propagation losses, weak light-matter interaction, and etalons; achieving 10-100 ppm precision at best. In 2024, the Photonic Sensing Group at UiT pushed down the CO_2 detection limits to a few ppbs, with thin film suspended SiN TM waveguides [1]. Yet, mid-IR absorption in those waveguides still limits their physical lengths to centimeters in shortwave mid-IR and completely obscures their transmission in the long-wave mid-IR, where most molecular fingerprints are located.

In this work, an innovative GeSi wall-like waveguide design and first experimental results will be presented. Compared to the suspended membrane structures, these are easier to manufacture and integrate with conventional photonic structures, allow more patterning flexibility, operate in TE polarization, and can be realized in materials transparent in full MIR range such as GeSi. The material choice provides compatibility with nonlinear components and fully integrated mid-IR sensors.

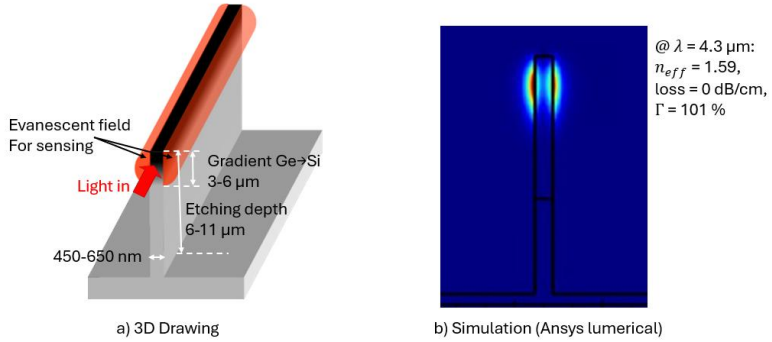

Figure 1 *(a) Schematic of the pillar waveguide and (b) the TE-mode distribution simulated using Ansys Lumerical.*

Fig. 1 shows an example of a wall waveguide design optimized for 4.3 µm, which maximizes the external confinement factor Γ (and therefore the interaction with the targeted gas species). It is realized as a 11 µm deep and 550 nm wide wall in a linearly graded GeSi platform [2] and theoretically achieves Γ > 100 % at 4.3 µm. Design considerations, fabrication protocols, and performance characterisations using a mid-IR spectroscopic setup at UiT will be presented.

References

[1] J. Salaj, M. Vlk, R. Zakoldaev, R.Seton, J. Čtyroký, S.Alberti, A.Aksnes, and J. Jágerská, *Suspended nanophotonic waveguide for isotope-specific CO_2 detection*, Optica 11, 1654-1662 (2024)
[2] J. M. Ramirez, V. Vakarin, J. Frigerio, P. Chaisakul, D. Chrastina, X. Le Roux, A. Ballabio, L. Vivien, G. Isella, and D. Marris-Morini, *Ge-rich graded-index $Si_{1-x}Ge_x$ waveguides with broadband tight mode confinement and flat anomalous dispersion for nonlinear mid-infrared photonics*, Opt. Express 25(6), 6561–6567 (2017).

Acknowledgments: This project receives funding from the European Union's Horizon Europe Research and Innovation Program (Grant No. 101128598, UNISON). The Research Council of Norway is also acknowledged for the support to the Norwegian Micro- and Nano-Fabrication Facility, NorFab.

POSTER-16 Dheerendra S Bhandari

Harnessing spin-orbit torque for electrical control of nanomagnets

Dheerendra S Bhandari,[1,*] Thea Marie Dale,[1] Akash Kumar,[2] Anders Strømberg,[1] and Erik Folven[1]

[1] *Department of Electronic Systems, Norwegian University of Science and Technology, Trondheim, Norway.*
[2] *Department of Physics, University of Gothenburg, Gothenburg, Sweden.*

Dipolar-coupled, interacting single-domain nanomagnets arranged in periodic or aperiodic lattices are commonly referred to as Artificial Spin Ice (ASI)[1, 2]. The freedom of geometrical arrangement provides a high degree of tunability in emergent behavior, rich magnetization dynamics, and nonlinear responses, positioning ASI as a promising platform for unconventional computing. In our recent work, we demonstrated that it is possible to achieve controlled, stepwise switching of individual nanomagnets within the ensemble by applying a global static magnetic field in carefully chosen directions[3]. However, despite this controllability, the reliance on global magnetic field input presents significant challenges for device applications, as it remains relatively slow and energy-intensive. The objective of this work is to employ the spin–orbit torque (SOT) mechanism as an electrical input for ASI systems[4, 5].

In this study, we focus on the type-XY SOT-driven switching mechanism, where the in-plane easy axis of the nanomagnets is tilted with respect to the current direction. This configuration enables field-free switching of the nanomagnets. This work establishes an electrical input scheme for in-plane ASI and to realise controlled, stepwise switching of the nanomagnet ensemble.

[1] S. H. Skjærvø, C. H. Marrows, R. L. Stamps, and L. J. Heyderman, Advances in artificial spin ice (2020).
[2] R. Sultana, A. K. Mondal, V. S. Bhat, K. Stenning, Y. Li, D. M. Arroo, A. Vasdev, M. R. McCarter, L. E. D. Long, J. T. Hastings, J. C. Gartside, and M. B. Jungfleisch, (2025).
[3] D. S. Bhandari, A. Strømberg, I. Breivik, A. Penty, J. H. Jensen, M. Foerster, G. Tufte, and E. Folven, Physical Review B **112**, 10.1103/qwx8-kkt9 (2025).
[4] Y. Takahashi, Y. Takeuchi, C. Zhang, B. Jinnai, S. Fukami, and H. Ohno, Applied Physics Letters **114**, 10.1063/1.5075542 (2019).
[5] Q. Shao, P. Li, L. Liu, H. Yang, S. Fukami, A. Razavi, H. Wu, K. Wang, F. Freimuth, Y. Mokrousov, M. D. Stiles, S. Emori, A. Hoffmann, J. Akerman, K. Roy, J. P. Wang, S. H. Yang, K. Garello, and W. Zhang, IEEE Transactions on Magnetics **57**, 10.1109/TMAG.2021.3078583 (2021).

* dheerendra.s.bhandari@ntnu.no

Selective Area Growth of GaN Nanowires on Si (111) with Ga Pre-Filling by Molecular Beam Epitaxy

Gulzhan Baigarinova, Tron Arne Nilsen, Swagata Bhunia, Helge Weman, and Bjørn-Ove Fimland

Dept. of Electronic Systems, Norwegian University of Science and Technology (NTNU), NO-7491 Trondheim, Norway
*E-mail: gulzhan.baigarinova@ntnu.no

Gallium nitride (GaN) nanowires have attracted significant attention due to their exceptional structural, optical, and electronic properties, making them promising candidates for advanced optoelectronic and power electronic applications. However, precise control over nanowire density, dimensions, and alignment remains a major challenge, as uncontrolled growth often results in non-uniform arrays that limit device performance. Selective area growth (SAG) is a powerful approach to achieve ordered nanowire arrays with well-defined geometries, which are essential for applications such as photonic crystals, light-emitting diodes, lasers, and single-photon sources. Despite its advantages, SAG of GaN nanowires on Si substrates patterned with SiO_2 masks is hindered by long nucleation times and parasitic growth. Conventional approaches typically rely on buffer layers, such as AlN or GaN templates, to improve selectivity. In this work, we propose an alternative buffer-free two-step growth strategy using plasma-assisted molecular beam epitaxy. In the first step, mask openings are pre-filled with a thin GaN layer at reduced temperature, forming preferential nucleation sites for subsequent nanowire growth. The results demonstrate that this approach significantly reduces nucleation time and overall growth duration while maintaining high selectivity. However, the intermediate annealing step, although effective in suppressing parasitic growth, partially degrades the initial nuclei, leading to the formation of multiple nanowires within a single opening. The reduced nucleation time enables a more reliable investigation of the SAG mechanism, allowing analysis of nanowire radius and length as a function of pitch without the influence of nucleation delay. The study highlights the critical role of pitch in determining nanowire morphology.

AFM Insights into Supramolecular Polymorphism of Chiral Amyloid Isoforms in Insulin and Lysozyme

Madhura B. Bonde,[1] Karsten Sættem Godø[2,3], Ayato Hanazawa[3], Takahiro Watanabe[3], Ulrik Prestmo[2,3], Hisako Sato[3], Tamotsu Zako[3], Mikael Lindgren[1], and Bjørn T. Stokke[1]

[1]*Dept of Physics, The Norwegian University of Science and Technology (NTNU), Trondheim, Norway*

[2]*Dept of Food Science and Biotechnology, The Norwegian University of Science and Technology (NTNU), Trondheim, Norway;* [3] *Dept of Chemistry and Biology, Ehime University, Matsuyama, Japan*

e-mail: madhura.b.bonde@ntnu.no

Supramolecular polymorphism of induced chiral amyloids of insulin and lysozyme studied using AFM. Formation of amyloid structures from different proteins is a common signature associated with neurodegenerative disorders as well as functional roles in other contexts. Recently, isoforms with distinct vibrational circular dichroism (VCD) signatures, categorized as left-, flat-, or right-handed chiralities, have been described. In this study, these three VCD isoforms of insulin and lysozyme were generated, verified by VCD, and examined by AFM to investigate possible structural polymorphism at the supramolecular level corresponding to VCD chirality. The isoforms were produced by inducing amyloid formation under varying pH conditions in aqueous solution [1]. Samples for AFM characterization were prepared by covalent immobilization on mica using a silanization method with carboxyl-terminated silanes, followed by conjugation to appropriate functional groups of the amyloid, like reported methods [2,3]. The samples were then vacuum dried and imaged using tapping mode AFM under ambient conditions. AFM topographs of right-handed insulin fibrils formed at pH 1.6 show fibrillar morphologies with variable lengths, significant lateral aggregation, and indications of twisted supramolecular structures. The left-handed insulin formed at pH 2.5 exhibits a lower tendency for extensive aggregation. Right-handed lysozyme amyloids formed at pH 2 display fibrils with nearly uniform thickness and minimal aggregation beyond the fibrillar state. The left-handed and flat lysozyme isoforms reveal additional variations in AFM morphology compared to the right-handed form. The most prominent differences in ultrastructure among the chiral amyloids studied arise from variations in supramolecular aggregation behavior between right-handed insulin and lysozyme (Fig. 1). Background CD data and fluorescence assays using chiral amyloid ligands will also be presented. The absence of clearly resolved chiral features in AFM suggests that VCD signatures originate from internal structural organization.

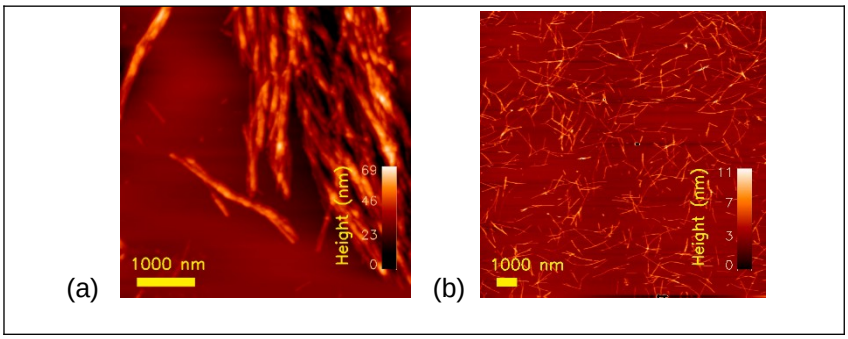

Figure 1: Tapping mode AFM topographs of VCD right-handed insulin amyloids (A) and VCD right-handed lysozyme amyloids.

References

1. Watanabe, T., et al., Chemphotochem, 2025. **9**(1).
2. Psonka-Antonczyk, K.M., et al., 2012. **13**(2): p. 1461–1480.
3. Schefer, L., et al., 2015. **7**(39): p. 16182–16188.

Influence of Ba-O Formation on Barium Titanate Thin Film Properties

D. Pulikkottil Dinesh*, O. Nilsen, H. H. Sønsteby
Department for Chemistry, Centre for Materials Science and Nanotechnology, University of Oslo, Norway

Barium titanate ($BaTiO_3$) is a key functional oxide for micro- and nanoelectronic applications, yet achieving reproducible thin film growth remains a persistent challenge. The sensitivity of barium-based chemistries, particularly the behaviour of Ba-containing precursors and intermediate Ba-O layers, plays a central role in determining final film properties

This work focuses on Ba-O thin film formation as a critical step toward controlled BTO growth. Processing conditions governing Ba-O film formation, stability and reactivity are systemically studied, with specific attention to air sensitivity and its consequences for downstream integration. These findings are used to guide Ba incorporation into BTO thin films, where compositional tuning is achieved through controlled variation of Ba content.

The resulting BTO films show clear dependencies of morphology and structural properties on Ba stoichiometry and processing conditions. Post-deposition treatments are found to further influence film quality, highlighting that both growth and subsequent processing steps matter. This work points to Ba-O chemistry as a key factor in controlling BTO thin film growth and offers insight into achieving reproducible compositionally tunable functional oxide films.

Patterning LSMO on Lithium Niobate for magnetomechanical devices

Authors: Marius Holen*, Johann Reimensberger, Erik Wahlström

Manipulating magnons with alternating electric and optical fields yields low conversion efficiency. Magnon coupling via phonons, using a magnetostrictive approach, has proven effective [1]. The magnanite LSMO is a ferromagnetic material with strong magnetostriction, where high magnon-phonon coupling efficiency has been demonstrated [2]. To generate the vibrations or phonons, LSMO is pulsed-laser-deposited (PLD) on lithium niobate (LN) to create a magnetostrictive hybrid structure that can be excited by appropriate electrodes. In our current projects, two types of device geometries are utilized: a surface acoustic wave (SAW) delay line and a nanomechanical resonator, both of which involve LSMO patterning at different length scales. Here, the results of the etching of LSMO for these purposes are presented.

For the SAW delay line, the resolution and roughness criteria are less demanding. Hence, wet etching can be used without affecting the LN substrate. Three candidates stand out in the literature: buffered hydrofluoric acid (BHF) [3], heated citric acid [4], and a mixture of HCl, KI, and ascorbic acid [5]. Only the first two are available etchants at NanoLab and were attempted here, while the latter may be introduced in the future. For the nanomechanical resonator, an extreme resolution of 50 nm or less is required. Here, an EBL mask and ion-beam etching (IBE) are used.

Wet etching of LSMO using BHF yields an etch rate of about 10 nm/min, but initial tests are not so promising. After hardbaking the resist, the selectivity is phenomenal at about 1:1. Heated citric acid also does not etch the resist, but it leaves behind leaching residue, making process optimization difficult. Dry etching using IBE looks promising, but requires further study. Removal of redeposition is done using BHF. An etch rate of 17 nm/min was measured. The selectivity with respect to the resist is slightly better than 1:1. In the future, we will also measure the sidewall angle, roughness and other material properties after etching. More results are expected before the conference, which will be included in the poster.

[1] Cassidy Berk et al., “Strongly coupled magnon–phonon dynamics in a single nanomagnet”, Nature Communications 10, 2652 (2019)

[2] Chunli Tang et al., “Tunable magnon-phonon cavity via structural phase transition”, arXiv:2510.06464 (2025)

[3] Joo-Hyung Kim et al., “Wet Etching Study of La0.67(Sr0.5Ca0.5)0.33MnO3 Films on Silicon Substrates”, J. Electron. Mater. 37, 361–367 (2008)

[4] Rajagopal et al., “Fabrication of La0.7Sr0.3MnO3–Si Heterojunctions Using a CMOS-Compatible Citric Acid Etch Process”, IEEE Electron Device Letters, vol. 32, no. 3, pp. 402-404 (2011)

[5] Dieter Weber et al., “Variable resistor made by repeated steps of epitaxial deposition and lithographic structuring of oxide layers by using wet chemical etchants”, arXiv:1301.4828v1 (2013)

4D X-ray imaging of NaCl crystal growth and morphology

Jessica Zeman*[1], Herborg Jess Sivilevičius[1], Giacomo Luani[1], Elvia Chavez Panduro[2], Dag Werner Breiby[1], Basab Chattopadhyay[1]

[1] *Department of Physics, Norwegian University of Science and Technology, Norway*
[2] *Department of Material Science, Norwegian University of Science and Technology, Norway*

Sodium chloride (NaCl) is one of the most common salts on Earth and is a primary example of a face-centred cubic (FCC) structure. Due to this geometry, NaCl typically forms flat-faced cubic crystals, as shown in Figure 1a. However, other morphologies such as dendritic, flat, and hopper crystals can form with certain impurities or under specific evaporation conditions.[1,2] Hopper crystals are characterised by a step-like structure (Figure 1b) and tend to form under high supersaturation, with diffusion limited crystal growth so the corners and edges form more quickly.[3] These situations are more likely in confined environments such as microcapillaries and small pore spaces.[1]

X-ray computed tomography (CT) can be a powerful technique to gain insights into how crystals form. As X-rays are attenuated by varying amounts depending on the material they are transmitted through, it is possible to get information on both the changing solution concentration and crystal structure during precipitation. In this poster we will show some of our resent results employing a fast 4D CT reconstruction technique[4] to gain new insights into the spatial and temporal growth of NaCl into hopper crystals and aggregates during evaporation at ambient conditions. Figure 1c shows the first few minutes of crystal growth after the first macroscopic crystals appear. At this early stage the crystals have more open spaces like hopper crystals and become more closely packed as the solution's saturation decreases.

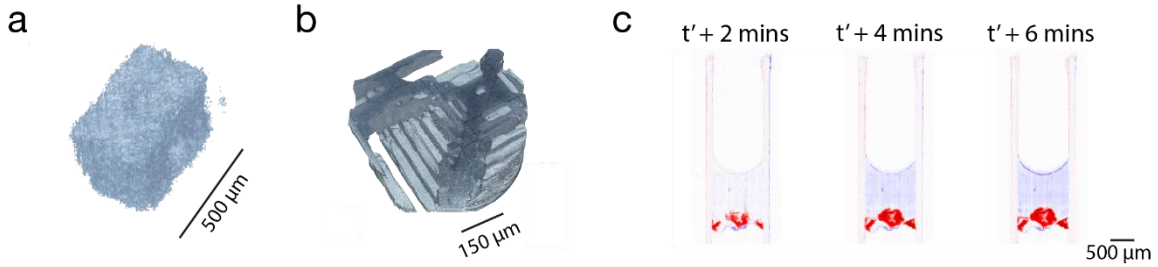

Figure 1 3D rendering from X-ray CT data of **a**) a typical flat-faced cubic NaCl crystal and **b)** a hopper crystal. **c)** Results from an X-ray CT experiment showing the first few minutes of crystal growth in a 2D slice as a difference image from *t'*, which is the time step just before the formation of the crystal.

Acknowledgements

The authors thank the Research Council of Norway for funding this research through the SaltyPore project (No. 335519).

References

1. Pettit, D. & Fontana, P. Comparison of sodium chloride hopper cubes grown under microgravity and terrestrial conditions. *npj Microgravity* **5**, 25 (2019).
2. Gupta, S., Pel, L., Steiger, M. & Kopinga, K. The effect of ferrocyanide ions on sodium chloride crystallization in salt mixtures. *Journal of Crystal Growth* **410**, 7–13 (2015).
3. Desarnaud, J., Derluyn, H., Carmeliet, J., Bonn, D. & Shahidzadeh, N. Hopper Growth of Salt Crystals. *J. Phys. Chem. Lett.* **9**, 2961–2966 (2018).
4. Friis, H. *et al.* Implicit neural representation for fast 4D computed tomography of multiphase flow in porous media. *Commun Phys* **8**, 339 (2025).

POSTER-22 Melania Rogowska

Atomic layer deposition of $BaSnO_3$ using novel metal-organic precursors: towards FeFET and FTJ integration.

*Melania Rogowska** *and Henrik Hovde Sønsteby*
Centre for Materials Science and Nanotechnology (SMN), University of Oslo

Conductive complex oxides are gaining increasing attention for next-generation oxide electronics, where stable and structurally compatible electrodes are essential. Among them, barium stannate ($BaSnO_3$, BSO) is a promising perovskite oxide due to its high room temperature carrier mobility, wide bandgap (~3.1 eV) enabling optical transparency, and excellent chemical and thermal stability. In addition, its ability to grow epitaxially on functional oxides such as $SrTiO_3$ (STO) and $LaAlO_3$ (LAO) enables high-quality heterostructure interfaces, positioning BSO as a candidate electrode material for ferroelectric field-effect transistors (FeFETs) and ferroelectric tunnel junctions (FTJs).

In this work, we investigate the atomic layer deposition (ALD) of BSO thin films using two novel chlorine-free β-diketonate precursors, $Ba(thd)_2$ and $Sn(thd)_2$ (thd = 2,2,6,6-tetramethyl-3,5-heptanedione), combined with ozone (O_3) as the oxidizing co-reactant. Film growth is achieved through a supercycle approach alternating BaO and SnO_2 subcycles. The Ba:Sn stoichiometry is tuned by varying the pulse ratio, enabling controlled formation of the perovskite phase. Film composition and stoichiometry are analyzed by X-ray fluorescence (XRF) and X-ray photoelectron spectroscopy (XPS), while crystallinity and phase formation are assessed by X-ray diffraction (XRD). The Ba:Sn ratio is directly correlated with the structural and chemical properties of the films.

We demonstrate the deposition of $BaSnO_3$ by ALD using chlorine-free precursors through precise supercycle control. This establishes a viable route to conformal, thickness- and composition-controlled BSO thin films for integration in oxide-based FeFET and FTJ device architectures.

POSTER-23 Joe Stickland

Coherent X-ray Diffraction Imaging of Microparticle Internal Morphology at Ultra-High Voxel Resolution

J. Stickland*[1], D. Younas[1], S. Ucar[2], Y. Chushkin[3], D. W. Breiby[1], B. Chattopadhyay[1]

[1]*Department of Physics, Norwegian University of Science and Technology (NTNU), Trondheim, Norway*

[2]*Department of Chemical Engineering, Norwegian University of Science and Technology (NTNU), Trondheim, Norway*

[3]*ESRF, The European Synchrotron, Grenoble, France*

**Corresponding Author: joe.stickland@ntnu.no*

Coherent X-ray diffraction imaging (CXDI) is a phase retrieval imaging method that reconstructs a real-space volume from the corresponding Fraunhofer (far-field) diffraction patterns [1]. The measured diffraction patterns of an object are directly related to the Fourier transform of the electron density of the sample. CXDI is a lensless imaging technique that retrieves the sample's structural information using the measured Fourier space amplitude and the iteratively recovered phase. The phase recovery algorithm alternates a prediction between real and Fourier spaces utilising known constraints [2]. These constraints are that the electron density must be positive and that we define a support region where the electron density is likely non-zero. The method, therefore, requires the sample to be isolated and the size to be constrained such that the resulting diffraction speckle size is sufficiently large to be oversampled by the detector. CXDI requires advanced, coherent X-ray sources, such as synchrotrons, in combination with state-of-the-art detectors and iterative phase retrieval algorithms [3].

CXDI is well-suited to image individual microparticles and we have primarily used the method to investigate the morphological development of calcium carbonate ($CaCO_3$) microparticles [4,5], an important constituent in shells and other exoskeletal structures [6]. We control the developing morphology of $CaCO_3$ through additives and the concentrations and confinement of precursors [7]. In this presentation, we will present an in-depth review of the CXDI methodology and demonstrate its use within the study of the 3D internal and external morphologies of a range of $CaCO_3$ particles with voxel sizes as up to 11 nm.

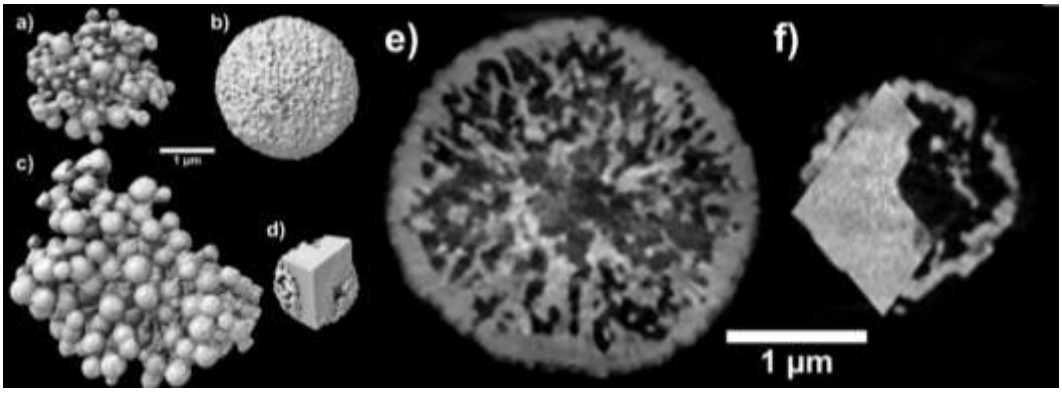

Figure: a)-d) Reconstructed electron density maps from CXDI of $CaCO_3$ particles formed with different concentrations of NaCl at different reaction times, a) 50 mM, 0 s; b) 50 mM, 300 s; c) 250 mM, 0 s and d) 250 mM, 300 s. e) and f) are the central slices of b) and d), respectively.

The authors would like to thank the Norwegian Research Council for financial funding through ICONIC (FRINATEK, project no. 303252) and the European Synchrotron Radiation Facility for the allocated beamtimes at ID10 through the proposals MA-5103, MA-5981 and MA-6938.

[1] Miao, J. et al. (2015). *Science* **348**(6234), 530
[2] Miao, J. et al. (1998). *J. Opt. Soc. Am. A* **15**, 1662
[3] Chushkin, Y., & Zontone, F. (2025). *IUCrJ* **2**(Pt 3), 280
[4] Younas, D., et al (2025) *APL Mater.* **13**(8), 081120
[5] Younas, D., et al (2026) *Phys. Rev. Research* **8**, 013051
[6] Weiner, S., & Addadi, L. (2011). *Annu. Rev. Mat. Sci.* **41,** 21
[7] Liendo, F., et al. (2022). *J. Crys. Gro.* **578**, 126406

POSTER-24 Tessana MASSE

A Thin-Film-Based Calibration Method for Quantitative Gradient Light Interference Microscopy

Tessana MASSE [1,], Komal Agarwal[1], Biswajoy Ghosh*[1]

[1]*Department of Physics and Technology, UiT-The Arctic University of Norway*
[*]*Presenting Author*

Department of Physics and Technology, UiT The Arctic University of Norway, Tromsø, Norway

Why this matters : Gradient Light Interference Microscopy (GLIM) is a label-free optical imaging technique that reveals detailed structures inside living cells without fluorescent dyes, making it ideal for long-term studies of biological processes. However, a major limitation is the lack of standardized calibration for optical path difference (OPD) measurements. OPD quantifies how much light slows down when passing through cells and is directly related to cell thickness and refractive index. Without accurate calibration, researchers cannot extract reliable quantitative data from GLIM images, limiting its applications in cell biology. This is particularly important for applications such as quantitative analysis of cell morphology and migration.

Goal : This work develops a simple and reproducible calibration method for GLIM using polymer thin-film reference standards.

Methods : Thin polymer films were fabricated to mimic relevant optical properties of biological samples, using multiple thicknesses and a range of refractive indices. Film thickness was measured using a profilometer with nanometer resolution, while refractive index was determined using ellipsometry. Theoretical OPD values for each reference sample were calculated using the relation $OPD = (n - n_0) \times$ thickness, where n is the refractive index of the material and n_0 is that of the surrounding medium. GLIM imaging of these reference standards is performed, and measured OPD values are compared with theoretical values to generate a calibration curve that converts raw GLIM signals into absolute OPD measurements.

Results : A complete set of reference samples has been fabricated, consisting of more than eight combinations of thickness and refractive index. A corresponding table of theoretical OPD values has been established, forming the basis for calibration.

Conclusion : This calibration protocol using polymer thin-film standards enables absolute OPD quantification in GLIM, making quantitative live-cell imaging more accurate and accessible. The method is simple and reproducible, while being robust enough for advanced cell biology applications.

Funding: We thank funding provided by the *MABIT-funded project -MarGel, UiT Talent project-Cymoplive, and the Research Council of Norway project- FiRsT.*

POSTER-25 Shubhankar Mishra

Designing RF Point Contact Spectroscopy: A Novel Modular Approach for Local Probing of Magnon-Phonon Coupling

Shubhankar Mishra *[1], Oleg Kurnosikov[2], Toshu An[3], Erik Wahlstrom[1]

[1] Department of Physics, Norwegian University of Science and Technology (NTNU), Trondheim, Norway

[2] Universite de Lorraine, Institute Jean Lamour, 54011 Nancy Cedex, France

[3] School of Materials Science, Japan Advanced Institute of Science and Technology (JAIST), JAPAN

Magnon-phonon coupling is essential for understanding hybrid excitations in magnetic materials and for developing next-generation magnonic and spintronic devices. Traditional techniques often lack sufficient spatial resolution or direct access to the local spectral function of the coupled modes.

We have designed and developed a custom **Radio-Frequency (RF) Point Contact Spectroscope** that enables direct, local investigation of magnon and phonon excitations through inelastic electron tunneling in a controllable nanoscale point contact. The instrument operates with broadband RF excitation (up to several GHz) and also measures the second derivative of the differential conductance (d^2I/dV^2) as function of bias voltage and RF to reveal the energy-dependent interaction spectrum.

Key features of the instrument:

- Mechanically stable point-contact probe with precise control over contact resistance (ballistic to diffusive regime)
- Low-noise RF generation, detection, and signal processing electronics
- Flexible sample stage compatible with thin films and bulk.
- Modular design with built-in provision for future integration into a cryostat.

At room temperature, the setup has been fully commissioned and initial measurements on selected graphite samples demonstrate clear spectral features corresponding to phonon excitations. The d^2I/dV^2 spectra show distinct peaks that can be attributed to the phonon density of states.

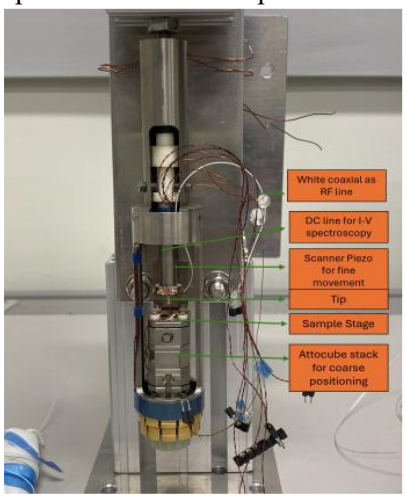

This RF point-contact approach offers high spatial resolution and local sensitivity. The modular architecture allows seamless transition from room-temperature characterization to low-temperature studies, where thermal broadening is minimized and hybrid magnon-phonon modes are expected to become more prominent.

Future low-temperature operation will enable detailed mapping of temperature- and field-dependent magnon-phonon hybridization, opening new avenues for quantitative studies of coupling strengths in novel materials such as van der Waals magnets and engineered magnonic structures.

1. Yanson, I. K. et al., Physical Review Letters, 95(18), 186602 (2005).
2. Balkashin, O. P. et al., Low Temperature Physics, 40(10), 929–934 (2014).
3. Wei, H. X. et al., Physical Review B, 82(13), 134436 (2010).
4. Liu, S. et al., Physical Review Letters, 127(9), 097401 (2021).

POSTER-26 Sudip Sharma

Surrogate-Based Multi-Objective Optimisation of Magnetic Induction Swing Adsorption Cycles for Post-Combustion CO_2 Capture

Sudip Sharma, Thomas A. Adams II*

Department of Energy and Process Engineering, Norwegian University of Science and Technology (NTNU), Trondheim, Norway

Post-combustion CO_2 capture via adsorption is constrained by the high energy penalty of fossil-derived steam regeneration. Magnetic Induction Swing Adsorption (MISA) replaces steam with inductive heating of ferromagnetic adsorbents, enabling fully electrified capture at rapid cycle times of 3–8 minutes—compatible with intermittent renewable electricity. This work presents multi-objective optimisation of four MISA cycle architectures for post-combustion capture from dried flue gas (15 mol% CO_2 in N_2) using Fe_3O_4@HKUST-1, a composite metal–organic framework combining high CO_2 uptake with ferromagnetic response for volumetric heating.

A one-dimensional fixed-bed model incorporating gas–solid mass and energy balances with local thermal non-equilibrium, Ergun momentum balance, linear driving force kinetics, competitive Binary Sips isotherm, and a dynamic wall energy balance is implemented in IDAES/Pyomo and validated against experimental breakthrough data ($R^2 > 0.996$). Since each cyclic steady-state simulation requires 35–60 CPU-minutes, a Gaussian Process (GP) surrogate (Matérn $\nu = 5/2$, ARD) replaces the IDAES simulator during optimisation. An active learning loop refines the surrogate against full IDAES validation, reducing Pareto-region prediction error by ~79% over three rounds. NSGA-II and MOPSO optimise the GP simultaneously, with anti-extrapolation guards ensuring prediction reliability.

Four cycle architectures of increasing complexity (5–12 design variables) are benchmarked (Fig. 1). Cycle A (3-step: Adsorption–Desorption–Cooling) achieves 68–82% purity and 59–81% recovery, fundamentally limited by N_2 co-desorption arising from comparable LDF mass transfer coefficients for CO_2 and N_2 on Fe_3O_4@HKUST-1. Cycle B (5-step, N_2 rinse) raises purity to 89.5% with up to 100% recovery but falls 0.5 percentage points short of the 90% CCU threshold due to N_2 carrier contamination—an architectural constraint irreducible by parameter tuning. Cycle C (5-step, CO_2 sweep) crosses the CCU barrier at 89–92% purity across 57–100% recovery. Cycle D (6-step, dual-stage inductive heating with dual recycle loops, 12 variables) achieves 95.6–98.0% purity with 57–100% recovery, simultaneously satisfying the CCS specification of ≥ 95% purity and ≥ 90% recovery.

Specific thermal energy ranges from 6.1 to 11.6 MJ/kg_{CO_2}— higher than zeolite 13X TSA (4.3 MJ/kg_{CO_2})—due to Fe_3O_4@HKUST-1's approximately 8× lower CO_2 working capacity. Under CCU constraints, Cycle D dominates Cycle C with 0.5–0.7 MJ/kg_{CO_2} lower energy at equal throughput. Under CCS constraints, only Cycle D produces feasible designs (9.0–10.4 MJ/kg_{CO_2}, 75–82 $kg_{CO_2}/(t_{ads} \cdot h)$. On low-carbon electricity grids, all MISA cycles outperform natural gas–steam TSA in net CO_2 avoidance, with a process-specific crossover grid intensity of 177 g/kWh for Cycle D–CCU. These results establish dual-stage inductive heating with recycle integration as essential for CCS-grade MISA performance.

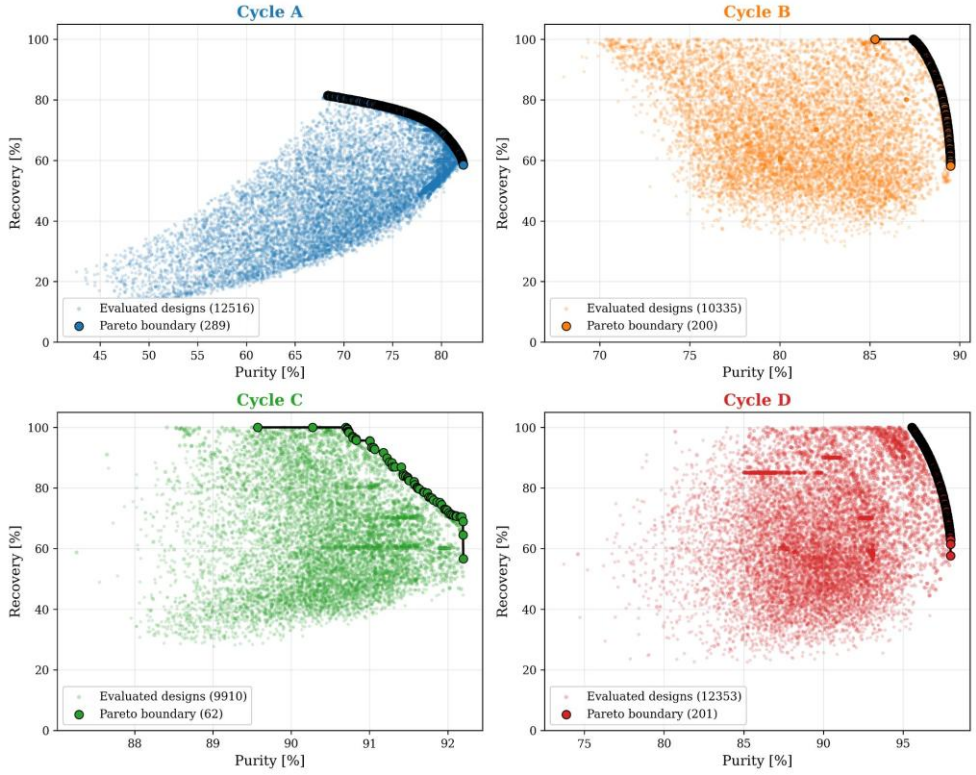

Fig. 1. Purity–recovery trade-off space for all four MISA cycle designs. Each panel shows surrogate-evaluated designs (scatter) and the NSGA-II Pareto-optimal boundary.

POSTER-27 Håvard Rugtvedt

Probing freezing-induced electrical potentials for novel energy harvesting from water

Håvard Rugtvedt[*,1], Erling Velten Rothmund, Yu Wei[1], and Senbo Xiao[1]
[1]NTNU Nanomechanical Lab, Department of Structural Engineering, Norwegian University of Science and Technology

For nearly 80 years it has been known that there is a transient electric potential across the ice–solution interface during ice growth in dilute aqueous solutions, caused by a selective incorporation of some ions into the bulk of the growing ice phase while others remain in the solution phase (*Figure 1*) [1,2]. Such a potential, referred to as a freezing potential, is distinguished from regular contact potentials by a several orders of magnitude size difference, with experimental values in the 100-300 V range being commonly achieved, capable of producing currents in the µA range [3-5]. The charge separation at the ice growing interface is driven by the thermal energy released during freezing of water—the latent heat of fusion—and is one form of energy that has so far not been utilised in energy harvesting applications. By high performance computational methods and experiments, this work probes the crucial steps in the buildup of the freezing potential at the nanoscale, aiming at identifying key thermodynamical and operational conditions for optimizing the freezing potential and the energy harvesting efficiency, exploring a new and renewable way of harvesting energy from water.

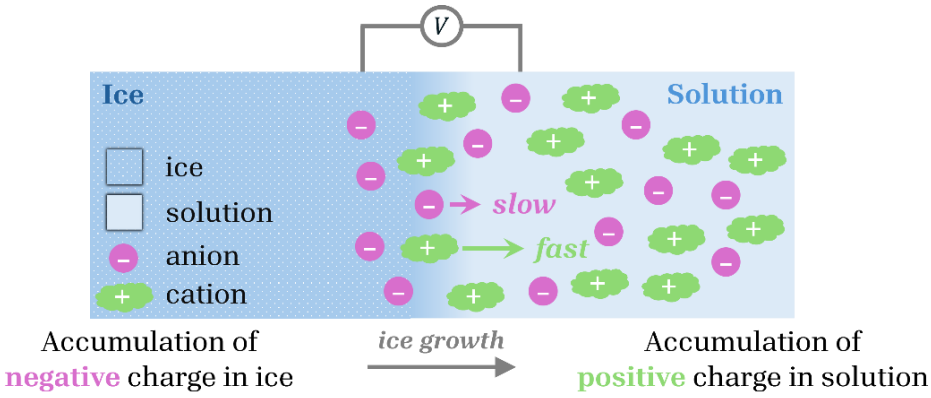

Figure 1: Schematic of the freezing potential mechanism. Because of a selective incorporation of anions over cations into ice during freezing, there is an accumulation of negative charge in the ice and of positive charge in the solution and a potential difference V between the two phases results.

References

[1] E. J. Workman and S. E. Reynolds. "A Suggested Mechanism for the Generation of Thunderstorm Electricity". In: *Phys. Rev.* 74 (1948), pp. 709–709. DOI: 10.1103/PhysRev.74. 709.

[2] G. W. Gross. "The Workman-Reynolds effect and ionic transfer processes at the ice-solution interface". In: *Journal of Geophysical Research* 70.10 (1965), pp. 2291–2300. DOI: 10.1029/JZ070i010p02291.

[3] E. J. Workman and S. E. Reynolds. "Electrical Phenomena Occurring during the Freezing of Dilute Aqueous Solutions and Their Possible Relationship to Thunderstorm Electricity". In: *Phys. Rev.* 78 (1950), pp. 254–259. DOI: 10.1103/ PhysRev.78.254.

[4] E. W. B. Gill. "Electrification by freezing". In: *British Journal of Applied Physics* 4 (1953). DOI: 10.1088/0508-3443/4/S2/ 306.

Drug Formulation and Mechanical Index Impacts Ultrasound-mediated Delivery of Doxorubicin in Tumors

Veronica Nordlund*[1,2], Sofie Snipstad[1,2], Sigrid Berg[3], Håkon F. Wesche[1], Caroline Einen Skjervold[4], Lovise Skåland[1], Anniken M. Sjødal[1,5], Catharina d. L. Davies[1,2]

[1]Department of Physics, Norwegian University of Science and Technology, Trondheim, Norway
[2] Cancer clinic, St. Olav's Hospital – Trondheim University Hospital, Trondheim, Norway
[3] Department of Health Research, SINTEF Digital, Trondheim, Norway
[4]Porelab and Department of Physics, Norwegian University of Science and Technology, Trondheim, Norway
[5]Department of Neurology, St. Olav's Hospital – Trondheim University Hospital, Trondheim, Norway
**Presenting author*

Treatment with focused ultrasound (FUS) in combination with the microbubble SonoVue has been shown to enhance both free drug and nanoparticle delivery in several preclinical works [1-3]. We previously showed that FUS treatment with a mechanical index (MI) 0.5 significantly increased the uptake of nanoparticles in the soft, well-vascularized murine colorectal tumor model CT26, but not in the stiffer, poorly vascularized murine pancreatic tumor KPC model [4]. We hypothesized that increasing the MI could improve delivery in the stiff KPC tumors. The transport of drugs is goverened by diffusion and convection, where diffusion is the main mechansim for small molecular drugs, whereas nanoparticles diffuse slowly and are depending on convection. Thus, the impact of FUS and microbubbles on drug delivery might be different for free and encapsulated drugs. More recently, low-MI sononeoperfusion has been proposed as an alternative approach to increase drug delivery to hypoperfused tumors [5, 6]. Therefore, we investigated the uptake of free and liposomal doxorubicin in CT26 and KPC tumors using SonoVue microbubbles and MIs ranging from 0 to 1.0.

Tumor cells from murine colorectal (CT26) and pancreatic (KPC) cancer were inoculated subcutaneously on the hind legs of mice for 12-21 days. Mice received free or liposomal doxorubicin (10 mg/kg) intraveneously before SonoVue injection and FUS exposure at MI 0, 0.3, 0.5, 0.8 or 1.0. Whole-animal fluorescence imaging quantified doxorubicin uptake before and after FUS. Five minutes before euthanasia, lectin-DyLight649 was injected to label functional vessels. Tumors were collected at defined timepoints (30 min, 4 h, 24 h). Additional groups receiving no drug were used to evaluate immediate perfusion changes after MI 0.3 and 0.5. Confocal microscopy quantified vascular function and drug microdistribution.

FUS treatment with MI 0.5 significantly increased the in vivo accumulation of liposomal doxorubicin in CT26, and there was a trend of higher and lower uptake in tumors treated with MI 0.3 and 0.8, respectively. In KPC tumors, FUS treatment with MI 0.3, 0.5 and 0.8 had no effect on liposomal doxorubicin uptake, and there was a trend of decreased uptake in tumors treated with MI 1.0. Reduced uptake at higher MIs might be due to vascular damage. FUS treatment with MI 0.3 had no impact on the uptake of free doxorubicin in either of the two tumor models, proably reflecting that free drug readily extravasate and diffuses through tumor tissue. Treatment with MI 0.3 and 0.5 did not significantly alter the perfusion immediately after treatment, with a trend of decreased perfusion, showing that sononeoperfusion was not induced. This was consistent with unaltered uptake of free doxorubicin after treatment with MI 0.3. Together, these results show that FUS + MB can increase the uptake of larger drug particles in well-vascularized tumors when choosing an MI that balances increased extravasation with vascular damage.

1.Haram, M., et al., *Ultrasound and Microbubbles Increase the Uptake of Platinum in Murine Orthotopic Pancreatic Tumors.* Ultrasound Med Biol, 2023. **49**(5): p. 1275–1287. 2. Snipstad, S., et al., *Sonopermeation Enhances Uptake and Therapeutic Effect of Free and Encapsulated Cabazitaxel.* Ultrasound Med Biol, 2021. **47**(5): p. 1319–1333. 3.Kotopoulis, S., et al., *Sonoporation-enhanced chemotherapy significantly reduces primary tumour burden in an orthotopic pancreatic cancer xenograft.* Mol Imaging Biol, 2014. **16**(1): p. 53–62. 4.Einen, C., et al., *Impact of the tumor microenvironment on delivery of nanomedicine in tumors treated with ultrasound and microbubbles.* Journal of controlled release, 2025. **378**: p. 656–670. 5.Zhang, Y., et al., *Sononeoperfusion effect by ultrasound and microbubble promotes nitric oxide release to alleviate hypoxia in a mouse MC38 tumor model.* Ultrason Sonochem, 2023. **100**: p. 106619. 6.Tang, N., et al., *Sononeoperfusion: a new therapeutic effect to enhance tumour blood perfusion using diagnostic ultrasound and microbubbles.* Cancer Imaging, 2023. **23**(1): p. 29.

POSTER-29 Enrico Melani

Thin-Film Lithium Tantalate for Nonlinear and Quantum Photonic Integrated Circuits

Author Enrico Melani

Supervisor Prof. Johann Riemensberger

NTNU - IES

Thin-film lithium tantalate (TFLT) is recently emerging as a promising platform for integrated photonics, offering a compelling combination of strong second-order nonlinearity (d_{33} = 14–27 pm/V), high electro-optical coefficient (r_{33} = 30.5 pm/V), wide transparency from 280 nm to 5000 nm, and enhanced resistance to photorefractive damage compared to its close relative lithium niobate (LN). These properties position TFLT as an attractive alternative to thin-film lithium niobate (TFLN) for scalable, wafer-level manufacturing of photonic integrated circuits (PICs) for both classical and quantum applications.

The central nonlinear process investigated in this work is optical parametric amplification (OPA), in which a strong pump wave at frequency ω_p transfers energy to a weaker signal at ω_s through the generation of an idler wave at ω_i, governed by energy conservation $\omega_p = \omega_s + \omega_i$. Achieving efficient OPA requires both a large nonlinear coefficient and phase matching between the interacting waves. When perfect phase matching cannot be obtained through dispersion engineering alone, quasi-phase matching (QPM) is implemented via periodic poling, which consists of periodically inverting the ferroelectric domain orientation by applying high-voltage electrical pulses through patterned electrodes. This inversion modulates the sign of d_{33} with a spatial period Λ, enabling efficient second-harmonic generation (SHG), difference-frequency generation (DFG), and OPA even in the presence of material and chromatic dispersion. Two distinct poling geometries are considered: periodic poling (PP) and layer poling (LP). While PP enables direct photon-pair generation by pumping at 775 nm, LP offers greater tolerance to geometric fabrication inaccuracies and potentially higher efficiency, at the cost of reduced accessibility of the required waveguide modes.

Device design is performed through numerical simulation of waveguide cross-sections, optimizing geometrical parameters to maximize modal overlap and satisfy phase-matching conditions between the pump and signal modes. Fabrication is carried out in the NTNU NanoLab cleanroom using electron beam lithography (EBL), reactive ion etching (RIE), ion beam etching (IBE), plasma-enhanced chemical vapour deposition (PECVD), and e-beam evaporation for electrode definition. Characterisation is then carried out to measure propagation loss and parametric gain, with the goal of validating simulated results and iteratively improving fabrication processes.

The long-term objectives are to explore the potential of the TFLT platform to achieve a key enabler for quantum communication, optical metrology, and next-generation coherent photonic systems.

[1] Wang, C. et al., “Lithium tantalate photonic integrated circuits for volume manufacturing,” Nature, 2024.

[2] Zhu, D. et al., “Integrated photonics on thin-film lithium niobate,” Adv. Opt. Photonics 13, 242–352 (2021).

[3] Zhang, M. et al., “Broadband electro-optic frequency comb generation in a lithium niobate microring resonator,” Nature 568, 373–377 (2019).

[4] Jankowski, M. et al., “Dispersion-engineered $\chi(2)$ nanophotonics,” J. Phys. Photonics 3, 042005 (2021).

[5] Gisin, N. and Thew, R., “Quantum communication,” Nature Photonics 1, 165–171 (2007).

[6] Chang, L., Liu, S. and Bowers, J. E., “Integrated optical frequency comb technologies,” Nature Photonics 16, 95–108 (2022).

[7] Chen, P.-K. et al., “Adapted poling to break the nonlinear efficiency limit in nanophotonic lithium niobate waveguides,” Nature Nanotechnology 19, 44–50 (2024).

POSTER-30 Ali Ghasemibousjin

High-Performance Broadband Infrared Silicon-based Doublet Metalenses Imaging: Evolution from Grayscale to One-Bit Binary Lithography(9-11 µm)

Ali Ghasemibousjin[1,2,3,4], Angelos Bouchouri[1,3,4], Dag Werner Breiby[3,4] , M. Nadeem Akram[1,3,4]
[1]Department of Microsystems, University of South-Eastern Norway, 3184 Borre, Norway [2]Smart Systems Integrated Solutions Consortium
[3]Department of Physics, Norwegian University of Science and Technology (NTNU), Høgskoleringen 5, 7491 Trondheim, Norway
[4]Email adress: 277128@usn.no, ali.ghasemibousjin@gmail.com, angelos.bouchouri@usn.no , muhammad.n.akram@usn.no, dag.breiby@ntnu.no

Abstract:

I. INTRODUCTION

Spheroids and traditional optical components for the broadband Long-Wave Infrared (LWIR) spectrum (8–12 µm) typically require bulky and expensive refractive lenses. Metasurfaces offer an ultra-compact alternative; however, designing achromatic metalenses for broadband operation remains a significant challenge due to severe chromatic dispersion. While previous efforts utilized grayscale lithography to encode phase via varying etch depths, this approach suffered heavily from Aspect-Ratio Dependent Etching (ARDE) and reactive-ion etching (RIE) lag during deep silicon etching, leading to severe phase deviations. This work presents the transition to a highly manufacturable "one-bit binary" lithography architecture to achieve broadband achromatic imaging.

II. METHODS

To completely bypass depth-control errors, our architecture utilizes silicon nanopillars with a strictly uniform etch depth of approximately 6–8 µm, modulating the optical phase entirely through varying the lateral dimensions. To achieve achromatic focusing at 9, 10, and 11 µm simultaneously, a comprehensive three-stream co-design pipeline was developed. First, Zemax OpticStudio was used to macro-design a Silicon Doublet, minimizing the chromatic dispersion gap of single lenses to extract ideal continuous phase profiles. Second, COMSOL Multiphysics was used to simulate a discrete library of four-fold symmetric meta-atoms consisting of four geometry families: solid squares, solid circles, solid crosses, and hollow squares. Finally, a custom Python-based Particle Swarm Optimization (PSO) algorithm was developed to map the continuous ideal phase profiles to the discrete multi-family library.

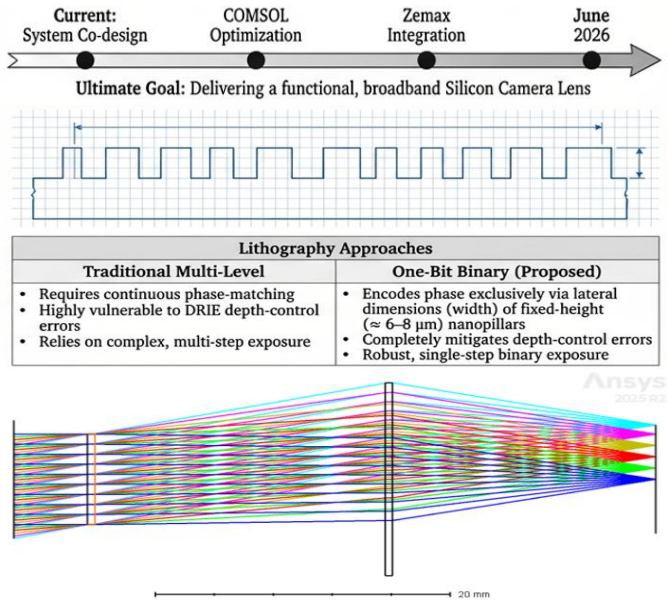

Figure 1 Doublet Configuration

I. RESULTS AND DISCUSSIONS

To Physical fabrication was conducted using maskless laser direct writing (Heidelberg DWL 66+) with an optimized dose of 100 mJ/cm² and the Deep Reactive Ion Etching (DRIE) Bosch process. An empirical engineering feedback loop revealed that highly dense or ultra-small features suffered from photoresist merging and severe DRIE scalloping. To resolve this, the meta-atom feature sizes were strictly bounded within a [1.0, 1.85] µm radius limit in the Python optimizer. Incorporating this physical constraint enabled the flawless structural transfer of all four geometry families into the final silicon substrate, including delicate structures like hollow squares.

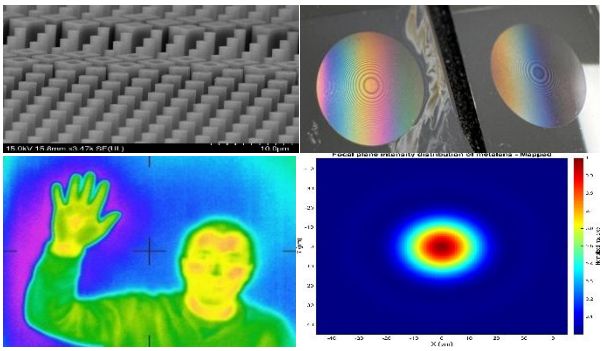

Figure 2 Four families meta-structures, B. Fabricated Singlet Lens for Multiple Wavelength, C. Thermal Image, D. Spot Diagram

I. CONCLUSION

By replacing depth-dependent grayscale geometries with a highly constrained, multi-family one-bit binary library, we successfully bridged the gap between theoretical optical system design and practical nano-fabrication. The PSO-driven pipeline mathematically and practically proves that broadband achromaticity (9–11 µm) is achievable in all-silicon doublets using standard maskless lithography, paving the way for compact, flat thermal imaging cameras.

Keywords—Metalens, Achromatic Imaging, Long-Wave Infrared, One-Bit Binary Lithography, Particle Swarm Optimization.

I. REFERENCES

[1] Y. Li, H. Huang, C. Zhang, X. Shang, Y. Liu, J. Hu, D. Shan, N. Tang, and W. Li, "Visible Light Broadband Achromatic Metalens Based on Variable Height Nanopillar Structures," Photonics, vol. 12, no. 1, Art. no. 31, Jan. 2025, doi: 10.3390/photonics12010031.

[2] X. You, R. Zhang, Z. Liu, H. Song, S. Li, and W. Huang, "Target-Driven Ring-by-Ring Optimization of an Achromatic and Coma-Corrected Long-Wave Infrared Hybrid Metalens for Large Field of View Imaging," IEEE Photonics Journal, 2026, doi: 10.1109/JPHOT.2026.3654923.

[3] J. G. George, S. Thomas, and S. Bhattacharya, "Design of multi-wavelength dielectric metasurfaces using finite element software," Asian Journal of Physics, 2021.

POSTER-31 Angelos Xomalis

NTNU
Kunnskap for en bedre verden

Pushing the limits of noninvasive health monitoring using nanophotonics

T. Steffensen[1], A. Torvund[2], V. Stubberud[3], J. Lövgren[2], N. K. Skjærvold[1,4], M. Steinert[3], A. Xomalis[2]
[1] Department of Circulation and Medical Imaging, NTNU, Trondheim 7030, Norway
[2] Nanoelectronics and Photonics Group, Department of Electronic Systems, NTNU, Trondheim 7034, Norway
[3] Department of Mechanical and Industrial Engineering, NTNU, Trondheim 7030, Norway
[4] St. Olav's University Hospital, Trondheim 7030, Norway
angelos.xomalis@ntnu.no

Continuous cardiovascular monitoring is essential for managing circulatory health and disease, yet most wearable sensors are constrained by reliance on electrical transduction and built-in electronics. We present a circuit-free, all-optical approach using diffraction from a skin-interfaced nanophotonic surface to detect minute skin strains from the arterial pulse. A smartphone camera records the shifting diffraction pattern in real time, removing the need for spectrometers or other optical hardware. In phantom and human studies, we recovered high-fidelity arterial pulse waves and detected benign arrhythmic events in close agreement with a clinical reference. Derived waveforms captured features linked to arterial stiffness, a key cardiovascular risk marker. Our approach uses battery-free, cost-effective, and disposable nanophotonic platforms enabling scalable monitoring for healthcare and broad consumer applications.

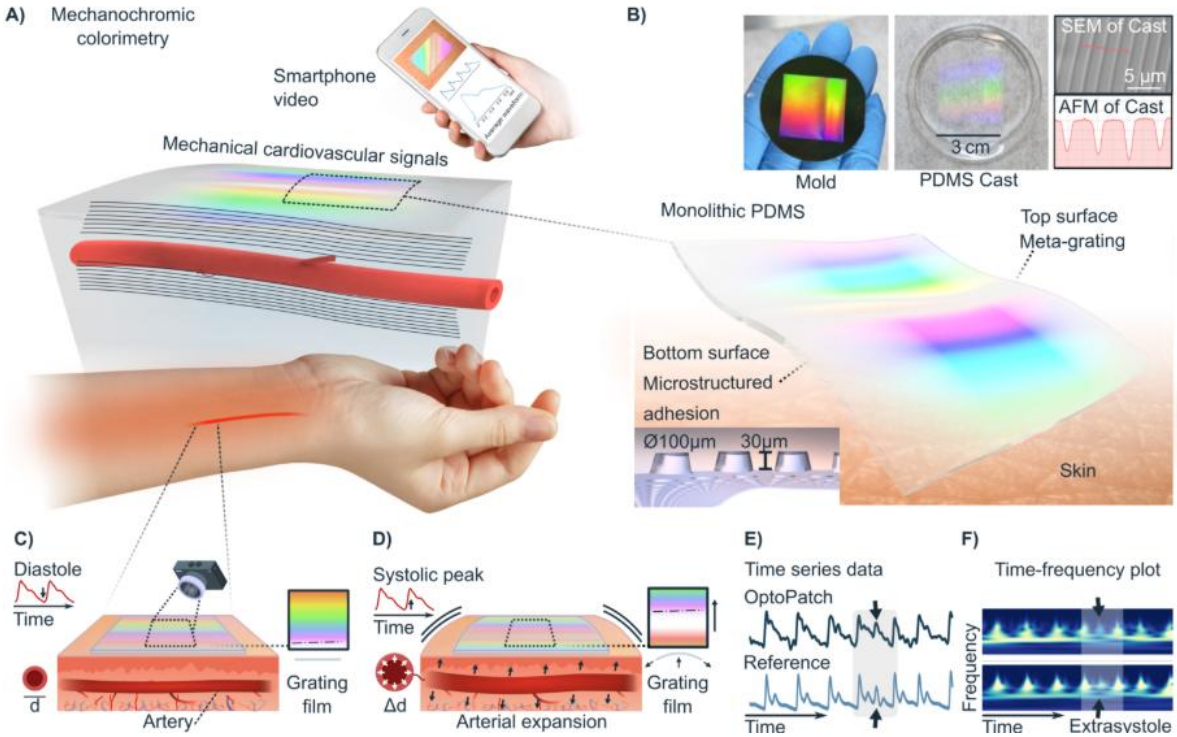

Figure 1: Concept of circuit-free cardiovascular monitoring via mechanochromic colorimetry. A) OptoPatch operating principle: a flexible nanophotonic meta-grating film adhered to the skin above the radial artery translates arterial expansion into diffraction colour shifts recorded by a smartphone camera. The underlying arterial anatomy is illustrated schematically. **B)** Device structure. Top: photographs of the nanofabricated mold (left) and resulting PDMS cast (right) with scanning electron microscopy (SEM) and atomic force microscopy (AFM) insets confirming surface-relief grating quality. Bottom: rendering of the monolithic PDMS film showing the meta-grating on the top surface and the microstructured suction-cup adhesive on the bottom surface (cavity diameter Ø100 µm, depth 30 µm), with the device conforming to skin. **C–D)** Working principle. During diastole (C), the artery is at baseline diameter and the grating film is relaxed; during systole (D), arterial expansion deforms the overlying film, shifting diffraction angles and the observed colour pattern relative to the camera pixels. **E)** Representative time-series data from OptoPatch (top) and a clinical non-invasive blood pressure (NIBP) reference (bottom) during an arrhythmic event (arrows). **F)** Normalized continuous wavelet transform (CWT) scalograms of the segment in (E) from OptoPatch (top) and NIBP (bottom), with arrows indicating the extrasystole event..